Retardation of Protein Dynamics by Trehalose in Dehydrated Systems of Photosynthetic Reaction Centers. Insights from Electron Transfer and Thermal Denaturation Kinetics

Retardation of Protein Dynamics by Trehalose in Dehydrated Systems of Photosynthetic Reaction Centers. Insights from Electron Transfer and Thermal Denaturation Kinetics.

Marco Malferrari, Francesco Francia, and Giovanni Venturoli

J. Phys. Chem. B 2015, 119, 13600−13618

Retardation of Protein Dynamics by Trehalose in Dehydrated Systems of Photosynthetic Reaction Centers. Insights from Electron Transfer and Thermal Denaturation Kinetics

Marco Malferrari[1], Francesco Francia[1], Giovanni Venturoli[1,2 *]

[1]Laboratorio di Biochimica e Biofisica Molecolare, Dipartimento di Farmacia e Biotecnologie, FaBiT, Università di Bologna, 40126 Bologna, Italy.

[2]Consorzio Nazionale Interuniversitario per le Scienze Fisiche della Materia (CNISM), c/o Dipartimento di Fisica, Università di Bologna, 40127 Bologna, Italy.

*Corresponding author. e-mail: giovanni.venturoli@unibo.it. Phone: 0039-051-2091288. Fax: 0039-051-242576

Abstract

Conformational protein dynamics is known to be hampered in amorphous matrices upon dehydration, both in the absence or in the presence of glass forming disaccharides, like trehalose, resulting in enhanced protein thermal stability. To shed light on such matrix effects we have compared the retardation of protein dynamics in photosynthetic bacterial reaction centers (RC) dehydrated at controlled relative humidity in the absence (RC films) or in the presence of trehalose (RC-trehalose glasses). Small scale RC dynamics, associated with the relaxation form the dark-adapted to the light-adapted conformation, have been probed up to the second timescale by analyzing the kinetics of electron transfer from the photoreduced quinone acceptor (Q_A^-) to the photoxidized primary donor (P^+) as a function of the duration of photoexcitation from 7 ns (laser pulse) to 20 s. A more severe inhibition of dynamics is found in RC-trehalose glasses as compared to RC films: only in the latter system a complete relaxation to the light-adapted conformation occurs even at extreme dehydration, although strongly retarded. To gain insight into the large scale RC dynamics up to the timescale of days, the kinetics of thermal denaturation have been studied at 44°C by spectral analysis of the Q_x and Q_y bands of the RC bacteriochlorin cofactors, as a function of the sugar/protein molar ratio, *m*, varied between 0 and 10^4. Upon increasing *m*, denaturation is slowed progressively, and above *m*~500 the RC is stable at least for several days. The stronger retardation of RC relaxation and dynamics induced by trehalose is discussed in the light of a recent molecular dynamics simulation study performed in matrices of the model protein lysozyme with and without trehalose. We suggest that the efficiency of trehalose in retarding RC dynamics and preventing thermal denaturation stems mainly from its propensity to form and stabilize extended networks of hydrogen bonds involving sugar, residual water, and surface residues of the RC complex and from its ability of reducing the free volume fraction of protein alone matrices.

Keywords: trehalose matrix, conformational dynamics, photosynthetic reaction center, thermal denaturation.

1. Introduction

Proteins can assume a large number of conformations which reflect their complex, rugged energy landscape.[1,2] At physiological temperature, anharmonic contributions to internal motions allow the protein to jump among different conformational substates, and often play an important role in protein reactivity and function.[3,4] Most of the information on the function-dynamics interplay has come from kinetic studies performed at cryogenic temperatures, which retard or arrest protein-specific motions, freezing the protein over selected ensembles of conformational substates (see e.g. ref. 5, 6). However, a drawback of this approach is that, to avoid the formation of ice crystals harmful to protein integrity, the temperature is lowered in the presence of co-solvents, as e.g. glycerol, forming amorphous solid matrices in which the protein is embedded.[7] Unfortunately, the effects of increasing the solvent rigidity and decreasing the temperature, both strongly affecting the dynamics of the matrix and of the protein,[7] are not easily disentangled. Insights into function-dynamics relationships have been also obtained by dehydrating the system at room temperature (see ref. 8 and references therein), since the activation of protein internal motions requires a minimum water content;[9] this procedure, however, often limits the structural stability of the protein.[10] An alternative to the above mentioned approaches consists in embedding the protein at room temperature into dehydrated amorphous matrices formed by disaccharides. Disaccharide glasses have been shown in fact to prevent damage due to external stresses, like dehydration and exposure to high or low temperatures.[11] Among sugars, trehalose (α-D-glucopyranosil α-D-glucopyranoside) exerts an extraordinary bioprotective action both *in vivo*, on tissues, cells, membranes and protein complexes,[11] and *in vitro,* on isolated biostructures.[12-14] Due to these properties, trehalose is increasingly used in pharmaceutical and biotechnological applications (see e.g. ref. 15, 16).

Although the molecular mechanisms of trehalose biopreservation are still controversial,[17,18] in the case of proteins it is established that the bioprotective action of trehalose stems from its ability of reducing the conformational dynamics when forming amorphous matrices at low water content. This was inferred from a number of experimental studies of protein-trehalose-water systems by

complementary techniques sensitive to atomic motion, including neutron scattering,[19,20] FTIR,[21] optical absorption,[22] Mössbauer,[22] EPR,[23] NMR[24], and X-ray absorption[25] spectroscopies. Additionally, molecular dynamics (MD) simulations of trehalose-water systems containing carboxymyoglobin (MbCO) have shown that (i) the amplitude of protein anharmonic motions is reduced in a trehalose matrix at low water content,[26] and (ii) structures are formed which confine the protein within a network of hydrogen bonds (HBs) connecting groups of the protein surface, water, and trehalose molecules.[27] The presence of water molecules bridging the protein surface with the trehalose matrix by means of multiple HBs, has been confirmed by a recent MD study performed on lysozyme-trehalose matrices.[28] On these bases it has been proposed that water-trehalose-protein structures play a role in the protein-matrix coupling determining protein stabilization (*anchorage* hypothesis).[29] The *anchorage* hypothesis, which emphasizes the role of multiple HBs at the protein matrix interface, incorporates some not mutually exclusive features of previous models, and, in this sense, it can be considered a generalization of the three main hypotheses previously formulated: (i) the *water replacement* hypothesis,[30] which postulates that stabilization is accomplished by the formation of HBs between the protein and the sugar; (ii) the *preferential hydration* hypothesis,[31] which suggests that the native protein structure is preserved by the residual water entrapped at the protein surface by formation of the glass; and (iii) the *high viscosity* hypothesis,[32] which focuses on the extraordinary viscosity increase upon vitrification. More recently, a prominent role of β relaxations in determining protein stability in sugar glassy matrices has been proposed, and evidence has been provided of a strong linear correlation between degradation rates and β relaxation times for different proteins embedded in a large number of antiplasticized sugar glass systems.[33]

In a series of works[23, 29, 34-36] we have shown that the incorporation into trehalose glasses of variable water content is a convenient approach to modulate at room temperature the dynamics of a large protein, the bacterial photosynthetic reaction center (RC), considered a paradigmatic system for studying function-dynamics relationships in electron transfer proteins. This integral pigment-

protein complex actuates a light-induced charge separation across the intracytoplasmic membrane, promoting the primary events of photosynthetic energy transduction.[37] The RC from *Rhodobacter (Rb.) sphaeroides* consists of three polypeptides: L, M and H. The L-M complex binds nine cofactors along two branches, related by a C_2 symmetry:[37] four bacteriochlorophyll (BChl), two bacteriopheophytin (BPheo) molecules, two ubiquinones (Q_A and Q_B) and a non-heme iron Fe^{2+}. Two of the BChl molecules, located on the periplasmic side of the complex, form an excitonic dimer ($BChl_2$), which, upon photoexcitation, acts as the primary electron donor P to the primary ubiquinone acceptor (Q_A), located on the opposite cytoplasmic side of the RC, generating within ~200 ps the primary charge separated state $P^+Q_A^-$. The photo-reduced Q_A^- in turn reduces the second ubiquinone molecule Q_B.[37] In the absence of electron donors to P^+, the electron on Q_B^- recombines with the hole on P^+. In Q_B deprived RC or in the presence of inhibitors of Q_A^- to Q_B electron transfer, charge recombination takes place by direct electron tunneling[38] from Q_A^- to P^+.

The RC conformational dynamics plays a role in most of the electron transfer processes which occur within the RC over different timescales.[6,39,40] We focused on the dynamics which stabilize the primary charge separated state $P^+Q_A^-$ by slowing its recombination. As shown by low temperature studies,[6, 41] this stabilization is brought about by the RC relaxation from a dark-adapted to a light-adapted conformation, which, at room temperature, occurs on a timescale shorter than 10^{-3} s. The two conformations differ in the rate of $P^+Q_A^-$ recombination (several times slower in the light- than in the dark-adapted conformation), and can be trapped by freezing the RC at cryogenic temperatures in the dark or under illumination.[6, 41] Furthermore, at low temperatures, the kinetics of $P^+Q_A^-$ recombination become strongly distributed in rate, due to RC trapping over a large ensemble of conformational substates, characterized by a different stability of the charge separated state.[6, 41] The kinetics of $P^+Q_A^-$ recombination after a short (ns) photoexcitation represent therefore a sensitive probe of the RC dynamics,[6, 42] reporting on the RC relaxation induced by the light-generated, intracomplex electric field, as well as on the thermal fluctuations of the RC among conformational substates over the timescale of this electron transfer process (10^{-2} s).

By this endogenous probe, we have shown that the RC relaxation which stabilizes the $P^+Q_A^-$ state, as well as the interconversion among conformational substates, can be strongly retarded at room temperature by incorporating the RC into dehydrated trehalose matrices. The hydration level of the glassy matrix tunes the internal RC dynamics, causing, under extensively dehydrated conditions, its complete block on the timescale of charge recombination, i.e. mimicking, at room temperature, the behavior of the hydrated system at cryogenic temperatures.[34, 43] Recently, we observed a comparable acceleration of $P^+Q_A^-$ recombination, after a pulsed photoexcitation, also in extensively dehydrated RC films, in the absence of trehalose.[44] This similarity might cast doubts on the actual role of trehalose in the retardation of protein dynamics. It has to be considered, however, that the comparably accelerated kinetics of $P^+Q_A^-$ recombination observed after a short (ns) flash in the absence and in the presence of trehalose, only indicates that the RC dynamics is arrested in both dehydrated matrices on the timescale of the electron transfer process used to probe conformational dynamics (10^{-2} s), without providing information on the effective extent and rate of the RC conformational relaxation on a longer time-window. We anticipated[44] that preliminary data suggested a stronger inhibition of the RC dynamics in the presence of trehalose. In the frame of the *anchorage* model, we proposed that a more effective hampering of RC conformational changes in the RC-trehalose matrix could be due to the formation of an extended HB network involving residual water molecules at the protein-matrix interface, RC surface groups and sugar molecules of the embedding matrix. Retardation of protein dynamics in dehydrated RC films was rather attributed[44] to the reduction of dielectric β relaxations of the whole protein matrix, dominated by the β fluctuation of the protein hydration shell[2], upon decreasing the content of residual water.

In the present paper we aimed at clarifying the role of trehalose in retarding or even suppressing conformational dynamics in dehydrated protein systems. To this end we have studied comparatively dehydrated amorphous RC systems formed in the absence or in the presence of trehalose. To probe RC dynamics involving different structural rearrangements on more extended timescales, we have examined: (i) the conformational RC relaxation induced by continuous

photoexcitation of increasing duration, up to 20 s, using an approach already exploited to probe the tightness of RC-matrix coupling;[35,36] (ii) the kinetics of thermal denaturation of the RC complex. Since the RC thermal stability was found to be dramatically enhanced in trehalose matrices at large (10^4) sugar/protein ratios, as compared to RC films dehydrated in the absence of sugar, we analyzed the dependence of isothermal denaturation kinetics upon the sugar/RC molar ratio. The results provide evidence that the small scale conformational dynamics associated with the stabilization of the charge separated state are retarded by dehydration in both amorphous systems on the second timescale, but are significantly more restricted in the presence of the sugar. Consistently with the notion that fast, small scale protein fluctuations are required to build up larger scale conformational rearrangements,[33, 45-49] the RC dynamics leading to thermal denaturation is also strongly retarded in dehydrated trehalose matrices as compared to RC films, the effect occurring already at low (10-10^2) sugar/RC ratios. These findings indicate a much stronger inhibition of the overall RC dynamics in the presence of trehalose, as previously proposed.[44]

2. Experimental Methods

2.1 RC purification and sample preparation

RCs were extracted from *Rb. sphaeroides* strain 2.4.1 membranes using lauryldimethylamine N-oxide (LDAO) as detergent, and purified as described in ref. 50. To prepare RC films, a drop (0.168 mL) of the RC-detergent suspension at 60 μM RC concentration in 10 mM Tris buffer, pH 8.0, in the presence of 10 mM o-phenanthroline (an inhibitor of Q_A^- to Q_B electron transfer) and 0.025% LDAO, was deposited on a 50 mm diameter CaF_2 window, and dried in a desiccator for about 4 hours under N_2 flow at room temperature. RC-trehalose amorphous matrices, characterized by a trehalose/RC molar ratio equal to $5\ 10^3$, were obtained by following a similar procedure from a drop (200 μL) of 50 μM RC in 10 mM Tris buffer, pH 8.0, 10 mM o-phenanthroline, 0.025% LDAO, and 250 mM trehalose. RC-trehalose glasses with different sugar/RC molar ratios (between 25 and 10^4) were obtained by keeping constant the total volume of the liquid drop and the RC

concentration, and by changing the trehalose concentration as appropriate. Trehalose (>99% purity) was used as supplied from Sigma-Aldrich.

The hydration of the RC film and RC-trehalose amorphous matrices was controlled by the isopiestic method described in detail in ref. 44: the window on which the RC film or RC-trehalose glass was formed, was inserted into a gas-tight sample holder containing saturated solutions of LiCl or P_2O_5 to obtain relative humidities at 297 K of 11% and 3% respectively.

2.2 Spectroscopic measurements and data analysis

FTIR measurements were performed using a Jasco Fourier transform 6100 spectrometer, with a DLATGS detector and a standard high-intensity ceramic source for the acquisition of spectra in the mid-IR region (7000-1000 cm^{-1}). Spectra extended to the NIR region (15000-2200 cm^{-1}) were measured with the same spectrometer, by using a halogen lamp source, and by replacing the Ge/KBr with a Si/CaF_2 beam splitter and the KRS-5 with a CaF_2 exit interferometer window. Visible-NIR absorption spectra were recorded on a Jasco V-550 spectrophotometer.

The content of residual water in the RC-trehalose matrices and RC films was estimated from the area under the NIR ($\nu_2 + \nu_3$) combination band of water at 5155 cm^{-1}, using an absorptivity value[51] of 102 absorbance unit nm M^{-1} cm^{-1}. We used the absorption band of the RC at 802 nm as an internal standard, as described in ref. 34, 44.

RC denaturation kinetics were obtained by incubating the RC films or RC-trehalose matrices inside a thermostated (accuracy ± 0.5°C) oven (M20-TB, MPM Instruments, Italy), the temperature of which was set to 50°C. The actual temperature of the sample during denaturation cycles was monitored continuously by a Pt100 ceramic resistance in contact with the CaF_2 window on which the RC film or RC-trehalose glass was formed. At the beginning of the denaturation cycle (t=0), when the sample was transferred from room temperature (24°C) inside the oven, a temperature of 44°C was reached with an half-time ~20 minutes. RC visible-NIR absorption spectra were recorded at room temperature at selected times during incubation. To this end the sample had to be removed from the thermostated oven, typically for 2 minutes, during which its temperature decreased by ~

4°C. As a consequence, between successive spectrophotometric measurements, the temperature of the sample varied between (42±1)°C and (46±1)°C. A time averaged incubation temperature of (44±2)°C was evaluated for the whole series of denaturation cycles.

Pulsed photoexcitation of RCs was accomplished by a frequency-doubled Q-switched Nd:YAG laser (Handy 710, Quanta System, Milano, Italy) delivering 95 mJ pulses of 7 ns width at 532 nm. Continuous illumination of RCs was provided by a 200 W quartz tungsten halogen lamp housed by a Oriel (Stratford, CT, USA) illuminator (model 66881). The polychromatic beam was filtered by 8 cm of thermostated water, by a long wave pass glass filter (cut-on wavelength at 750 nm), and focused by a condenser at the entrance of an optical fiber bundle, the output of which was collimated on the sample. The flux on the sample was 740 Wm^{-2}. The duration of photoexcitation was varied between 5 ms and 20 s using a Uniblitz electro-programmable shutter (Vincent Associates, Rochester, NY, USA), with a closure time equal to 300 μs.

The recombination kinetics of the light-induced $P^+Q_A^-$ state were recorded at 422 nm, using an optical bench for time-resolved absorption spectroscopy of local design.[29] When photoexciting by continuous light the photomultiplier was protected from the scattered actinic light by a 10^{-4} blocking, 10 nm bandwidth interference filter centered at 420 nm and by a Corning 4-96 glass filter (cut-on wavelength at 600 nm). When using the pulsed laser photoexcitation, the photomultiplier was additionally screened by a holographic notch filter centered at 532 nm. From 4 to 64 kinetic traces were averaged depending on the required time-resolution and signal-to-noise ratio. During averaging the sample was allowed to dark adapt for at least 1 min between successive photoexcitations. All kinetic measurements were performed at 297 K.

Fitting of $P^+Q_A^-$ recombination to model kinetics and decomposition into Gaussian bands of the RC NIR spectrum were performed by least-squares minimization routines based on modified Marquardt and grid search algorithms[52] using locally developed software. Confidence intervals of fitting parameters were evaluated numerically as described in detail in ref. 43.

3. Results

3.1 Dehydration of the RC-trehalose matrices under controlled relative humidity.

Exposure to an atmosphere of definite relative humidity, obtained by gaseous equilibration with different saturated salt solutions, is a suitable method to control the hydration level of protein films.[44,53] In RC films, formed by small amounts of RC-detergent complexes (about 1 mg), at relative humidity *r* between 95% and 3%, hydration equilibrium is reached in a few hours.[44] Figure 1 demonstrates that this isopiestic method can be used also to control the hydration of amorphous RC-glasses, although in this case equilibrium is reached only in a few days. Figure 1A shows the time course of the water content of a RC-trehalose matrix during incubation at *r*=11%, followed by further dehydration at *r*=3%, and rehydration upon re-exposure at *r*=11%. An enlargement of the initial kinetics is plotted in Figure 1B. After vitrification, samples have been immediately exposed (at *t*=0) to *r*=11%. The water content reaches a steady level of ~ 0.47 H_2O per trehalose molecule in ~ 200 h. Incubation at *r*=3% (starting at *t*=800 h) results in a further drying, down to ~ 0.04 H_2O per trehalose molecule. When the dehydrated sample, at *t*=1288 h, is again equilibrated at *r*=11%, a water content of ~0.44 H_2O per trehalose molecule is reversibly restored, indicating that equilibrium is reached during the first incubation at *r*=11%.

3.2 The kinetics of $P^+Q_A^-$ recombination following continuous photoexcitation: a comparison between amorphous RC systems in the presence and in the absence of trehalose.

The kinetics of $P^+Q_A^-$ recombination following a short (ns) laser photoexcitation of RCs is a sensitive probe of the RC conformational dynamics involved in the relaxation from the dark- to the light-adapted state. In sufficiently dehydrated RC-trehalose matrices,[29,34] as well as RC films,[44] the $P^+Q_A^-$ recombination after a pulsed ns photoexcitation is accelerated at room temperature by a factor of ~5 as compared to solution, indicating that the RC relaxation is essentially blocked on the timescale of charge recombination (see Introduction and section 4.2 of Discussion). The retardation of RC dynamics can be probed on a longer timescale by analyzing the kinetics of $P^+Q_A^-$ recombination after continuous photoexcitation of increasing duration. In RC from *Rb. sphaeroides*

R26, incorporated into dehydrated trehalose glasses, we observed, in fact, that increasing the duration of photoexcitation from a few milliseconds to a few seconds results in progressively slower recombination kinetics, indicating that, during continuous illumination, a partial relaxation and stabilization of the $P^+Q_A^-$ state occurs.[36] Following this approach, we have now compared the kinetics of $P^+Q_A^-$ decay after continuous illumination in RC-trehalose glasses and in RC films.

The kinetics recorded after a laser pulse and after 20 s of continuous photoexcitation in RC-trehalose matrices and RC films equilibrated at the same relative humidity, *r*=11%, are shown in Figure 2 (panel A and B, respectively), together with the kinetics measured in solution after the laser pulse. The $P^+Q_A^-$ decay following the short (7 ns) laser photoexcitation is strongly accelerated, as compared to solution, in both amorphous systems. In line with previous reports,[29,34,36,43] the decays after the laser pulse can be fitted to a power law

$$N(t) = \frac{\Delta A_{422}\,(t)}{\Delta A_{422}\,(0)} = (1 + \lambda t)^{-n} \qquad (1)$$

where *N(t)* is the survival probability of the $P^+Q_A^-$ state, which is supposed to be described by a continuous distribution *p(k)* of first-order rate constants *k*, according to

$$N(t) = \int_0^\infty p(k)\, exp(-kt) dk \qquad (2)$$

By taking the inverse Laplace transform of *N(t)*, it can be shown that, when *N(t)* obeys eq.1, *p(k)* is a Gamma distribution, i.e.

$$p(k) = \frac{k^{n-1} exp(-k/\lambda)}{\lambda^n \Gamma(n)} \qquad (3)$$

where Γ(n) is the Gamma function. The best fitting parameters λ and *n* determine *p(k)*, yielding in particular the average rate constant, <*k*>, and the variance σ^2 of the distribution, given by

$$\langle k \rangle = n\lambda \qquad \text{and} \qquad \sigma^2 = n\lambda^2 \tag{4}$$

Kinetic analysis yields <*k*>=38.6±0.4 s^{-1} and σ=21.6±0.4 s^{-1} in the RC-trehalose matrix, as compared to <*k*>=11.4±0.3 s^{-1} and σ=1.94±0.4 s^{-1} in solution RCs (Fig.2A). Errors are given within two standard deviations. In the RC film, dehydration also leads to a strong acceleration of the kinetics (Fig.2B), which, as already observed,[44] includes, besides the kinetic component in the 10 ms timescale, described by eq.1, an additional distributed kinetic phase, in the hundreds of microseconds timescale, accounting for about 47% of the total decay. The faster component, described by an additional power law (<*k*>=1520±420 s^{-1}, σ=1530±680 s^{-1}), has been attributed to a subpopulation of RCs from which the more tightly bound water molecules have been removed, causing structural distortion and/or alteration of the thermodynamic parameters (free-energy change, reorganization energy) which govern the rate of electron transfer.[44] The average rate constant (<*k*>=34.0±2.5 s^{-1}) and the rate distribution width (σ=26.0±5.4 s^{-1}) of the slower component in the RC film are very close to those determined in the RC-trehalose matrix, as it is also evident from the corresponding rate distributions (see the insets of Fig.2 A and B). Comparably large values of <*k*> and σ have been measured in water-glycerol RC systems only at cryogenic temperatures.[6,41,54,55] It appears therefore that, following a single charge separation event, the RC relaxation from the dark- to the light-adapted conformation is strongly hampered at room temperature, either in the presence or in the absence of trehalose. Over this timescale (10^{-1} s) not only the relaxation, but also interconversions among RC substates, are strongly retarded in both dehydrated matrices, as indicated by the large broadening of the rate distributions (insets of Fig.2 A and B).

Fig.2 shows that, at variance, after a prolonged (*Δt*=20 s) photoexcitation, the kinetics of $P^+Q_A^-$ recombination are markedly different in the presence and in the absence of trehalose. In both systems continuous illumination, as compared to laser pulse photoexcitation, leads to a slower kinetics. The effect is however very limited in the RC-trehalose glass (Fig.2A), where <*k*>

decreases from 38.6±0.4 s^{-1} to 25.4±0.2 s^{-1}. On the contrary, in the RC film, the prolonged photoexcitation results in a much slower recombination kinetics, characterized by $<k>$=10.2±0.2 s^{-1}, a value coincident, within the experimental error, with that measured in solution RCs. Interestingly, the kinetics retain however a significant non-exponential character (σ=7.4±0.4 s^{-1}), which corresponds to a rate distribution much broader than in solution RCs (inset of Fig.2B) and in an overall lifetime of $P^+Q_A^-$ even longer than in solution, due to the contribution of the slowly decaying components.

The different response of RC-trehalose glasses and RC films to continuous illumination is further documented in Figure 3, which shows the dependencies of $<k>$ and σ upon the duration of the continuous photoexcitation, Δt, in the two amorphous systems, equilibrated at the same relative humidity r=11%. For comparison, values of $<k>$ and σ determined in solution RCs are also plotted. They do not depend upon Δt over the range examined (7 10^{-9} s - 20 s).

In the RC-trehalose glasses the average rate constant decreases progressively when Δt increases from 5 ms to ~100 ms (Fig.3A, open squares). For longer illumination times $<k>$ levels to a value more than two-times larger than that measured in solution. The width of the rate distribution follows an analogous behavior (Fig.3B). The described Δt dependence of $<k>$ and σ indicates that, although the probability that the photoexcited RC relax from the dark- to the light-adapted conformation is very low in the dehydrated trehalose matrix (as shown by the fast kinetics recorded following a pulsed photoexcitation), continuous illumination lasting for hundreds of milliseconds allows the relaxation of the system into a conformation which significantly stabilizes the charge separated state, as compared to the dark-adapted conformation. The RC complex embedded into the dehydrated trehalose matrix is however unable to attain the light-adapted conformation accessible in solution, even after a continuous photoexcitation lasting 20 s, since the minimum $<k>$ value obtained under these conditions is more than two-times larger than the one measured in solution. The decrease of the rate distribution width σ at increasing Δt suggests additionally that, during

continuous photoexcitation, as a consequence of the increased time spent in the charge separated state, the RC is gaining some internal mobility, partially averaging the rate distribution (see Discussion).

In the RC film, a steeper decrease of <*k*> and σ is observed upon increasing *Δt* (Fig. 3A, filled circles). Noteworthy, at *Δt* >1 s the value of <*k*> coincides with that measured in solution RCs, showing that the effect of dehydration on the average rate constant for $P^+Q_A^-$ recombination measured after a laser pulse can be totally reverted by a sufficiently long pre-illumination of the system. As shown in Fig. 3B, after such a prolonged photoexcitation (*Δt* >1s), the width of the distribution reaches a steady value (σ≅6 s^{-1}), lower than that attained in the trehalose glass (σ≅14 s^{-1}), but still larger than that in solution RCs (σ ≅ 3 s^{-1}), indicating that, in the absence of trehalose, the continuous photoexcitation increases to a larger extent the conformational mobility of the RC, without, however, totally suppressing the kinetic heterogeneity.

A difference in the response to continuous light between RC amorphous matrices in the presence and in the absence of trehalose is also detectable, although less pronounced, when the systems are brought to extreme dryness through equilibration at *r*=3%. Figure 4 shows that, under these more dehydrated conditions, <*k*> and σ determined after a laser pulse have increased, as compared to the less dehydrated matrices (*r*=11%), both in RC-trehalose glasses[43] and in RC films[44], reaching values comparable to those measured in aqueous systems only at T < 70 K.[55] When the RC-trehalose matrix is preilluminated by continuous light of increasing *Δt*, <k> and σ decrease progressively and reach essentially the same steady values determined at *r*=11%, well above those measured in solution RCs. In the RC film, on the contrary, the <*k*> value characteristic of RC solutions (≅10 s^{-1}) is reached following prolonged illumination, in spite of the extreme dehydration. This occurs only at *Δt* > 10 s, as compared to *Δt* > 1 s at *r*=11% (see Fig.3A), suggesting a more restricted RC mobility under extreme dryness. Interestingly, at *r*=3%, the decrease of σ at increasing *Δt* is similar in the RC-trehalose matrix and in the RC film (Fig.4), in

line with an increased inhibition of the interconversion among conformational substates in the more dehydrated RC film.

3.3 RC thermal stability in dehydrated films and trehalose matrices at high sugar/RC molar ratio.

The results of section 3.2 indicate that, although the relaxation of the photoexcited RC is strongly retarded in both RC films and RC-trehalose glasses, in the absence of trehalose the RC retains a significantly larger degree of internal mobility. This conclusion holds for the conformational changes which take place during continuous illumination between 10^{-3} and 10 s. This RC relaxation, stabilizing the $P^+Q_A^-$ state, most likely involves small-scale rearrangements.[56-59] Thermal stability studies can provide complementary information on larger-scale, longer-time internal motions. The loss of the native structure at high temperature is thought in fact to imply structural changes affecting the tertiary RC structure, and occurring on longer time-windows, e.g. 10^3 s in solution RC at 48 °C.[60]

We have performed a systematic analysis of the kinetics of RC denaturation at 44 °C, in dehydrated RC films and in a set of RC-trehalose glassy matrices in which the sugar/RC molar ratio was varied over a large range. The approach previously used to obtain isothermal denaturation kinetics, based on the time evolution at high temperature of the NIR spectrum of the RC bacteriochlorin cofactors,[29,60,61] has been improved by analyzing also the Q_x spectral region, and resolving in the NIR spectrum the contributions of the BChl and BPheo molecules released from their binding pocket during denaturation.

The NIR spectrum of the native RC can be decomposed into four Gaussian bands[29,61] (Figure 5A), centred at ~860 nm (band 1), ~800 nm (band 2), and ~760 nm (band 3), principally assigned to the low energy exciton component of the Q_y transition of the special-pair bacteriochlorophylls ($BChl_2$), to the Q_y transitions of the two monomeric BChls, and of the two BPheos, respectively. The assignment of the small band at ~680 nm (band 4) is uncertain.[61] Studies in RC-detergent solutions[60], in RCs reconstituted into phospholipid vesicles,[61] and incorporated into amorphous sucrose matrices,[29] have shown that the exposure to high temperature induces the progressive

decrease of the BChl bands at ~860 nm (band 1) and ~800 nm (band 2), accompanied by an absorption increase between ~740 and ~770 nm. The decrease of bands 1 and 2 indicates that $BChl_2$ and monomeric BChls bound to the RC lose their native environment. The absorbance increase between ~740 and ~770 nm may be due to the conversion to pheophytin (peaking at ~760 nm) of bound BChls and/or to the release of BChls and BPheos from their binding pockets, since BChl and Bpheo in organic solvents show absorption maxima at ~770 and ~750 nm, respectively.[62-64]

Figure 5 shows the NIR spectrum between 650 and 950 nm recorded at selected times during incubation of 44 °C of a RC-trehalose matrix (panel A) and of a RC film (panels B-D). Both samples have been dried at r=11% in the presence of a saturated LiCl solution. When a steady content of residual water was reached (~2.5 10^3 and ~900 water molecules per RC, in the presence and absence of trehalose, respectively), samples were rapidly transferred under N_2 flow to new holders which were filled only with dry nitrogen and sealed before starting (at t=0) incubation at high temperature. The hydration of the samples remained essentially constant during incubation.

The spectrum of the RC embedded in trehalose does not change appreciably, even after 96 hours of incubation at 44°C (Fig. 5A), indicating that the sugar matrix fully preserves the native structure of the pigment binding sites. On the contrary, as shown by panels B, C, and D, the spectrum of the RC film undergoes progressive alterations, diagnostic of the RC denaturation: a decrease of the bands at ~860 nm and ~800 nm occurs already after exposure at 44°C for 2 hours (panel C), and becomes more pronounced after 7 hours (panel D). The weakening of these bands, ascribed to the dimeric $BChl_2$ and monomeric BChl native state, is paralleled by an absorption increase between ~740 and ~770 nm. Whether the latter absorption change reflects pheophytinization of the RC bound BChls or the loss of BChl and BPheo native coordination, can be distinguished by examining the spectral changes observed in the region of the Q_x bacteriochlorin transitions. In fact, in the Q_x region of the intact RC, the bound BChls, irrespective of their dimeric ($BChl_2$) or monomeric state, give rise to a single band at 597 nm, well separated from that

originating from the bound BPheos, centered at 534 nm (Figure 6). Loss of the central magnesium atom from the BChls will therefore cause an increase of the latter band, at the expenses of the BChl band at 597 nm. The spectra of Figure 6 shows that this is not the case: incubation at 44°C for 7 h does not affect significantly the relative amplitudes of the BPheo and BChl Q_x bands, which are only slightly attenuated. Even after a more prolonged incubation at 44°C, up to ~ 13 days, the ratio of the areas underlying the Q_x BPheo and BChl bands remains essentially constant (see Table 1), indicating that no significant conversion of BChl into BPheo takes place during denaturation of the RC. Rather, as shown by Figure 6, incubation for 7 h causes a blue shift of BPheo and BChl Q_x bands, as well as of the bands due to the carotenoid (spheroidenone) bound to the RC, peaking at 505 nm and 471 nm in the intact complex. The peak wavelengths of the Q_x transitions of the RC cofactors in RC films are plotted in Figure 7 (black symbols), panel A (BChl and BPheo) and B (carotenoid), as a function of the incubation time at 44°C. The Q_x bands of all the cofactors undergo a systematic, progressive blue shift. The peak wavelength of the BChl band reaches at t>50 h a steady value (585 nm), shifted towards the peak (576 nm) of BChl in petroleum ether RC extracts[62]. Correspondingly, the BPheo band maximum shifts from 534 nm (at t=0 h) to 526 nm (at t>50 h), a value very close to that of the BPheo band in petroleum ether RC extracts (524 nm) .[62] The peaks of the carotenoid bands are shifted (at t>20 h) by 9 and 11 nm respectively, again towards the peak wavelengths measured in organic solvents.[63] As a whole, the changes observed in the Q_x spectral region indicate that the BChl, BPheo, and carotenoid molecules lose their native environment within the RC.

In the light of the above conclusions, the kinetics of RC denaturation in the RC film were analyzed by decomposing each NIR spectrum, $A(\lambda)$, recorded at time t during incubation, into 6 Gaussian bands. Besides the four bands required to describe the Q_y region of the intact RC (see Fig.5B), centred at ~860 nm ($BChl_2$ dimer, band 1), ~800 nm (monomeric BChls, band 2), ~760 nm (BPheos, band 3), and ~700 nm (band 4), two additional bands were included, corresponding to the

contribution of BChl (band 5) and BPheo (band 6) released by the RC. For each spectrum the absorbance A as a function of the wavelength λ was fitted to

$$A(\lambda) = \frac{1}{\sqrt{2\pi}} \sum_{i=1}^{6} \frac{A_i}{\sigma_i} exp\left[-\frac{(\lambda - \lambda_i)^2}{2\,\sigma_i^2}\right] \qquad (5)$$

with the areas A_i underlying each band i, and the corresponding widths σ_i as adjustable parameters. In order to reduce the number of parameters, the peak wavelengths of the bands due to the released BChl and BPheo (λ_5 and λ_6) were fixed to 770 nm and 750 nm, respectively, i.e. to the values determined in organic solvents. The peak wavelengths of monomeric BChls and BPheos bound to the RC (λ_2 and λ_3), close to those of the released pigments, were also fixed (± 1 nm) to the values measured in the intact RC, i.e. to 802 nm and 757 nm, respectively, while the positions of the two bands at the extremes of the spectral region, λ_1 ($BChl_2$) and λ_4, were allowed to be adjusted within the interval (835-860 nm) and (690-708 nm), respectively. The best fitting procedure yielded λ_1 values fluctuating around 842 nm by ± 4 nm for the different spectra analyzed, while λ_4 was systematically centered at 690 nm. Representative examples of the decomposition into 6 Gaussian bands are given in panels C and D of Figure 5.

The areas of band 1, 2, and 5 are plotted in Figure 8 A, B, and C as a function of the incubation time of the RC film. As expected, the area of band 1 (at 842 ± 4 nm) and of band 2 (802 nm), proportional to the concentration of bound $BChl_2$ and monomeric BChls, respectively, decrease upon increasing the time of incubation at high temperature, while the area of band 5 (770 nm), proportional to the concentration of unbound BChl, increases. During the release of bound BChls, the area of band 3 (757 nm, bound BPheo) decreases, and the area of band 6 (750 nm, unbound BPheo) increases (not shown), indicating that also BPheos are losing their native environment. The uncertainties on A_3 and A_6 of the latter bands, as evaluated from the confidence intervals of the best fitting parameters (see Experimental Methods), are significantly larger than those of bands 1, 2 and 5, presumably due to the considerable overlapping of bands 3 and 6. We

have therefore based the quantitative analysis of the denaturation kinetics on the time evolution of the areas of bands 1, 2 and 5 (Figure 8). To this end, and to further test the consistency of the described spectral decomposition, the following minimum kinetic scheme has been considered

$$(BChl_2) \overset{k_1}{\rightarrow} (unbound\ BChl) \overset{k_2}{\leftarrow} (monomeric\ BChl) \qquad (6)$$

where *(BChl₂)* and *(monomeric BChl)* refer to $BChl_2$ and accessory BChls, bound to the RC. Their concentration is assumed proportional to A_1 and A_2, respectively. The BChl released from the RC binding pockets, (*unbound BChl*), is assumed to contribute to A_5, and k_1 and k_2 are pseudo-first-order rate constants (see Discussion). Under these assumptions, the following time evolution is expected for A_1, A_2, and A_5:

$$A_1(t) = A_1(0)[(1 - f_1)exp(-k_1 t) + f_1] \qquad (7)$$

$$A_2(t) = A_2(0)[(1 - f_2)exp(-k_2 t) + f_2] \qquad (8)$$

$$A_5(t) = A'_5\{(1 - f_1)[1 - exp(-k_1 t)] + (1 - f_2)[1 - exp(-k_2 t)]\} \qquad (9)$$

where f_1 and f_2 have been introduced to account for the small fractions of bound *(BChl₂)* and *(monomeric BChl)*, respectively, which, as shown in Figure 8 A and B, are not released by the RC on the timescale examined. The parameter A'_5, which determines the asymptotic value of A_5 for $t \rightarrow \infty$, depends upon the integrated absorption coefficient of *(unbound BChl)*. Eqs.7-9 describe well the time dependence of A_1, A_2 and A_5, obtained from the decomposition of the NIR spectra, as shown by the continuous lines in Figure 8A-C. The experimental values $A_1(t)$ and $A_2(t)$ have been fitted to eq. 7 and 8, with $A_1(0)$, k_1, f_1 and $A_2(0)$, k_2, f_2 as free parameters. When fitting $A_5(t)$ to eq.9 (panel C) the only adjustable parameter was A'_5 , since k_1, k_2, f_1 *and* f_2 were already determined by the previous fit to eq. 7 and 8. The agreement between fit and experimental values provides therefore a rather strict test of consistency of the model. The value obtained for A'_5 (9.0 ± 0.5 nm), when compared with those of $A_1(0)$=(9.3 ± 0.3) nm and $A_2(0)$=(9.7 ± 0.5) nm, implies that the integrated absorption coefficients for the bound and for the released BChsl are similar. As shown by

the comparable values of k_1 and k_2 (see the legend of Figure 8), the release of $BChl_2$, bound at the P site of the primary electron donor, is essentially concomitant with the release of the two accessory BChls from the symmetrical binding pockets.

Summarizing, the glassy trehalose matrix is extremely more effective in inhibiting the dynamics which leads to RC denaturation than the amorphous protein-detergent dehydrated film, in which the characteristic time of thermal denaturation is about 4 hours.

3.4 What is the minimum trehalose/protein molar ratio required to fully preserve the RC integrity at high temperature ?

The RC-trehalose matrices so far examined were characterized by a sugar/protein molar ratio, *m,* equal to 5 10^3; under these conditions the volume of the disaccharide matrix exceeds that occupied by the embedded protein (see Discussion). In view of the substantially different thermal stability of RC in the protein alone and protein-trehalose matrix with such a large *m* value, we have studied the dependence of the denaturation kinetics in RC-trehalose matrices as a function of the sugar/RC molar ratio, from m=25 to m=10^4. We aimed at defining the minimum sugar/RC molar ratio which prevents thermal denaturation at 44°C on the timescale of days.

Denaturation kinetics at *m* values between zero (RC films) and 200 have been obtained by decomposing the NIR spectra of the RC bacteriochlorins, as described in detail above for the case of the RC film. The area of band 1, 2 and 5 are shown in Figure 9A, B and C as a function of the incubation time. To better compare the kinetics observed in the different RC-trehalose glasses and in the RC film, the areas of bands 1 and 2 at each time of incubation have been normalized to the area of the respective bands at t=0 h. For each *m* value, the areas of band 5 have been normalized to the sum of the corresponding area of band 1 and of band 2 at t=0 h. For each set of data (i.e. for each *m* value) continuous lines represent best fit to eqs. 7-9, modified according to the described normalization. The values obtained for the kinetic parameters are summarized in Table 2. As already observed in the case of the RC film, also for the RC-trehalose matrices, the decay kinetics of the areas A_1 and A_2 are consistent with the kinetics of appearance of band 5. For $0 < m \leq 200$ the

denaturation kinetics are very sensitive to the sugar/protein ratio. The presence of a very low number of trehalose molecules per RC (m=25) already induces a detectable slowing in the release of $BChl_2$ (panel A) and of the monomeric BChls (panel B), as compared to the RC film. Upon increasing the trehalose/RC molar ratio up to m=200, both k_1 and k_2 decrease markedly (see Table 2), indicating that the thermal stability of the RC is progressively and strongly increased. Interestingly, in the presence of trehalose, for $0 < m \leq 200$, the decay of A_2 is generally slower than that of A_1; additionally, the ratio between the rate constants k_1 and k_2 of A_1 and A_2 decay tends to increase with m. This behavior suggests that, in the presence of an increasing number of trehalose molecules per RC, the release of the monomeric BChls is increasingly hindered as compared to that of $BChl_2$.

At $m \geq 500$ no significant alteration can be observed in the NIR spectra even after 5 days at 44°C; at these molar ratios, the sum of four Gaussian bands, corresponding to the contributions of the bound bacteriochlorin cofactors only, well accounts for the spectra (see Figure 5A for m=5 10^3). Accordingly, as shown in Figure 9 (panel A and B) A_1 and A_2 do not depend (within the experimental uncertainty) upon the time of incubation. At $m \geq 500$, by taking into account the experimental error and the maximum time of incubation explored, an upper limit for the rate constant of BChl release around 10^{-3} h^{-1} can be set conservatively. Consistently, at m=5 10^3, no alteration of the NIR spectrum was detected even after 20 days incubation at 44°C (not shown).

The conclusions drawn from the data of Figure 9 are corroborated and complemented by the time dependence of the blue shift of the carotenoid and of the Q_x bacteriochlorin bands observed in RC-trehalose glasses (Figure 7). Consistently with the analysis of the Q_y bacteriochlorin bands, the presence of only 25 trehalose molecules per RC significantly slows also the time course of the blue shift of BChl and BPheo Q_x bands (Figure 7A), as well as that of the carotenoid bands (Figure 7B). At m=200, the BChl and BPheo release is drastically slowed, and that of the carotenoid blocked.

Thermal denaturation analysis at 44°C shows therefore that above a threshold value close to 500 trehalose molecules per RC the associated internal dynamics is blocked on the timescale of

several days, and that, when the trehalose/RC ratio is decreased below this threshold, the constraints which hamper large scale RC dynamics are progressively weakened.

4. Discussion

4.1 Kinetics of water exchange between RC-trehalose matrices and atmospheres of controlled relative humidity.

Gaseous equilibration with saturated salt solutions, providing appropriate values of relative humidity *r*, allows to control accurately and reversibly the hydration of RC-trehalose glasses (Fig.1). In matrices characterized by a sugar/protein molar ratio m=5 10^3, equilibration at r=11% yields a hydration level (~0.47 H_2O/trehalose) which compares well with that (0.52 ± 0.03) determined in binary trehalose-water matrices at the same r.[65] Therefore, at high m values, the presence of the protein has a negligible effect on the affinity for water of the matrix. At r=3%, residual water can be further reduced to about 1 water per 25 sugar molecules.

The much longer dehydration/re-hydration times required for equilibration in RC-trehalose matrices, as compared to RC films,[44] reflect clearly the large contribution to hydration of trehalose, and are in line with MD simulations, comparatively performed, at low hydration levels, on amorphous matrices, formed by (i) the model globular protein lysozyme, (ii) pure trehalose, and (iii) a lysozyme/trehalose mixture.[28] This study revealed that the stiff trehalose matrix sterically hinders the exchange of H-bonds between water molecules, and makes water less mobile in the trehalose-protein matrix than in the matrix formed by the protein alone.

Dehydration/rehydration kinetics can be described by exponential decay/recovery (black lines in Figure 1). A significantly better fit is provided however by stretched exponential (red lines in Figure 1), especially in the case of the initial dehydration phase at r=11% (see Figure 1B), i.e.

$$y(t) = [y(t_0) - y(t_\infty)]exp\left[-((t - t_0)/\tau)^\beta\right] + y(t_\infty) \quad (10)$$

and

$$y(t) = y(t_0) + [y(t_\infty) - y(t_0)]\left\{1 - exp\left[-((t - t_0)/\tau)^\beta\right]\right\} \quad (11)$$

for dehydration and hydration, respectively, where *y(t)* represents the (H_2O/trehalose) molar ratio at time *t*, t_0 is the initial time of dehydration/rehydration, and $0 < \beta \leq 1$. Non-exponential kinetics have been observed in different polymeric and amorphous systems for sorption/desorption processes not simply controlled by the energetics of surface attachment/detachment, but rate limited by different transport mechanisms, including diffusion.[66-69] It has been pointed out that for diffusion limited processes the sorption/desorption kinetics are well accounted for by a stretched exponential, and that the exponent β may be related to the geometry of the system.[66,68] The analysis of dehydration/rehydration kinetics support a diffusion limited water exchange between the RC-trehalose matrix and the atmosphere.

4.2. $P^+Q_A^-$ recombination kinetics following continuous photoexcitation: probing the retardation of the RC conformational relaxation up to the second time scale.

Dehydration of RCs both in the absence[44] or in the presence[43] of a trehalose matrix results in a several-fold accelerated and largely distributed kinetics of $P^+Q_A^-$ recombination following a short (ns) laser photoexcitation. To rationalize these effects we adopted a conceptual framework, schematized in Figure 10, originally introduced by Nienhaus and coworkers[6] to analyze the coupling between electron transfer and RC dynamics. The model accounts for the temperature dependence (5-300K) of $P^+Q_A^-$ recombination kinetics in native[6] and genetically modified[55] RCs, dispersed in water-glycerol, as well as entrapped in a sol-gel matrix.[42] To discuss the results of the continuous photoexcitation experiment (section 3.2), we summarize here the main features of the model. Figure 10 depicts overall parabolic, highly rugged, free energy surfaces of the $P^+Q_A^-$ state and of the PQ_A ground state as a function of a conformational coordinate q, which defines (at q=0) a dark-adapted conformation (D), and (at q=1) a light adapted conformation (L). Transitions between the neutral and charge-separated states are represented by vertical arrows (Frank-Condon approximation), and the rate constant of the nonadiabatic electron transfer is governed by the energy gap, E(q), which contains the reaction free energy and the reorganization energy associated with the slow degrees of freedom mapped on q. The charge separated state is stabilized in the L

conformation, as compared to D, since the energy gap E is smaller at q=1 than at q=0. Following a short light excitation of dark-adapted RCs (q=0), the system jumps to the upper surface, where it remains before charge recombination. The ability of the system to relax from D to L, by performing diffusive motions on the $P^+Q_A^-$ surface, depends on the ruggedness of the energy landscape, i.e. on the size of the energy barriers between protein conformational substates, and on the thermal energy of the system. At room temperature, the RC relaxes from q=0 to q=1 during the lifetime of $P^+Q_A^-$ which recombines from the stabilized L conformation (path 1 in Figure 10). Upon decreasing thermal energy, motion on the $P^+Q_A^-$ surface becomes slow on the timescale of charge recombination, and electron transfer occurs from partially (path 2) or even totally (path 3) unrelaxed conformations, resulting in a faster $P^+Q_A^-$ recombination kinetics. The static conformational heterogeneity of the RC is sketched by the distributions centered over the minima of the free energy surfaces. At room temperature, the RC rapidly samples this conformational ensemble, and almost exponential kinetics are observed. At cryogenic temperatures thermal fluctuations are arrested resulting in a large distribution *p(k)* of rate coefficients (see eq. 3), It follows that recombination kinetics probe the RC conformational dynamics on the scale of $P^+Q_A^-$ lifetime: the average rate constant, $\langle k \rangle$ probes the relaxation from D to L, while the width σ of *p(k)* reports on the rapidity of interconversion between substates.

The $\langle k \rangle$ and σ values obtained from the kinetics of $P^+Q_A^-$ recombination after a laser pulse in RC films and in RC-trehalose glasses at low relative humidity (Figure 3 and 4) are in excellent agreement with previous measurements, in which the dependence of these parameters on hydration was systematically studied.[43,44] The large increase of $\langle k \rangle$ observed at room temperature upon dehydration is comparable to that observed in glycerol-water upon decreasing the temperature from 200 to 50 K:[55] $\langle k \rangle$ values very close to those measured at r=3% in the RC film ($\langle k \rangle$=44 s^{-1}) and in the RC-trehalose glass ($\langle k \rangle$=52 s^{-1}) have been determined in water-glycerol mixtures at T≅100K and T≅50K respectively.[55] We infer that the RC relaxation in essentially blocked at room temperature in the most dehydrated amorphous matrices on the timescale probed by charge

recombination (10^{-1} s). Consistently with such a strong inhibition, dehydration results in a large broadening of the rate distribution function (Figure 3B and 4B), indicating that the interconversion between the substates of the D conformation is also arrested. The overall behavior observed at room temperature upon dehydration implies a large increase, in both amorphous RC systems, of the ruggedness of the free energy surfaces of Figure 10.

The kinetic analysis of $P^+Q_A^-$ recombination following continuous photoexcitation allows in principle to probe the RC relaxation on a longer timescale. We expect, in fact, that, if the system is maintained on the $P^+Q_A^-$ surface by continuous photoexcitation for a sufficiently long time Δt, even in the presence of high energy barriers, it can eventually evolve along q, relaxing slowly towards the L conformation. The extent of relaxation along q will be measured by the average rate constant of $P^+Q_A^-$ recombination after the continuous photoexcitation.

The dependence of $\langle k \rangle$ upon the duration Δt of continuous illumination in dehydrated RC films and RC-trehalose glasses (Figure 3A and 4A) shows that relaxation along q takes place in both amorphous systems between 10^{-2} s and 10 s. However, the extent and rapidity of relaxation differ in the presence or in the absence of trehalose. In the RC film, even under the most dehydrated conditions (r=3%), the system attains in a few seconds of continuous illumination a light-adapted conformation L, which is as stable as in solution, suggesting that the energy gaps E(q), at q=0 and q=1, are not significantly changed as compared to solution, and that dehydration causes, in the absence of trehalose, mainly an increase of the energy barriers separating conformational substates. At variance, only a slower and partial relaxation is observed in the RC-trehalose glass, indicating that, in the presence of trehalose, dehydration causes a larger alteration of the energy landscape, due to strong protein-matrix interactions.

In RC films, complete stabilization is reached for $\Delta t > 1$s at r=11%, and for $\Delta t > 10$ s at r=3%. This suggests that the ruggedness of the energy surfaces is further increased when the number of residual water molecules per RC is decreased from ~900 (at r=11%) to ~80 (at r=3%),[44]

in line with a significant "lubricating" effect of water belonging to the hydration shell of the complex.

In the case of RC-only matrices, the detected residual water is most likely bound to the RC-detergent complex.[44] At variance, in the presence of sugar, it is expected that the residual water molecules are not homogeneously distributed within the RC-trehalose matrix, but rather associated preferentially with the RC complex, due to the exclusion of trehalose from the surface of proteins in the presence of water.[70,71] Indeed the preferential exclusion of trehalose from contact with the protein surface, shown for concentrated sugar solutions, has been extended also to the solid state by MD simulations performed in glassy trehalose systems incorporating MbCO[27] or lysozyme.[28] In the latter study it was found that in strongly dehydrated lysozyme-trehalose glasses, at 0.075 g of H_2O/g of protein, (47±2)% of the total residual water molecules formed bridges between the protein surfaces and trehalose molecules. Although the larger size of the RC, as well as the larger sugar to protein molar ratio in our protein-trehalose system, can affect the water distribution within the matrix, a rough estimate based on the above fraction of water molecules interacting with lysozyme, yields 1105±85 residual water molecules associated with the RC-detergent complex in RC-trehalose glasses equilibrated at r=11% and characterized by 5 10^3 trehalose molecules per RC (see Figure 1). Since a number of ~ 900 water molecules per RC has been determined in RC-films at the same relative humidity,[44] the above estimate suggests a comparable size of the residual RC hydration layer in the RC films and RC-trehalose matrices used in continuous light experiments. At r=3% a similar evaluation yields for RC-trehalose glasses (94±47) RC-associated water molecules, as compared to ~80 determined in RC films.[44]

The distribution width, σ, carrying information on the rapidity of the RC thermal fluctuation among conformational substates, also evolves upon increasing Δt (Figure 3B and 4B). The kinetics recorded after the ns laser photoexcitation yields broad, comparable distributions in dehydrated RC films and RC-trehalose glasses, consistent with a similar static RC heterogeneity in the absence and

in the presence of the sugar. In both amorphous matrices, σ increases from ~25 s^{-1} at *r*=11% to ~37 s^{-1} at *r*=3%, suggesting, in agreement with the similar dependence of <*k*>, a more effective inhibition of RC dynamics under the most dehydrated conditions.

Interestingly, upon increasing the duration *Δt* of continuous illumination the rate distribution narrows, and σ reaches a minimum value for *Δt*≈1 s and *Δt* >20 s at *r*=11% and *r*=3%, respectively. Under both hydration levels, and for both amorphous matrices, the minimum σ values are always significantly larger than in solution, where the distribution is very narrow (σ≈2 s^{-1}). According to the dynamic model of Figure 10, the narrowing of the rate distribution reflects a faster interconversion between conformational substates, leading to averaging of the static RC heterogeneity over the timescale of charge recombination.[6, 34, 42] We propose that the attempts of the system to relax along the *q* coordinate during continuous photoexcitation, cause transient, local collapses of the constraints which retard RC dynamics. These constraints are thought to stem from HB networks involving the residual water molecules, the RC complex and, in the case of the RC-trehalose glasses, the sugar matrix (see below). Such an interpretation implies that the ruggedness of the $P^+Q_A^-$ energy surface is reduced to some extent during continuous illumination, possibly facilitating the hindered relaxation along *q*. This agrees with the less pronounced narrowing of the rate distribution, symptomatic of a larger impairment of conformational dynamics, observed at *r*=11% in the RC-trehalose glass as compared to the RC film. In the latter system weaker constrains are indeed expected, as judged from the ability of the RC to fully relax from D to L under continuous light. At *r*=3% a more limited narrowing of the rate distribution, occurring at larger *Δt*, is detected also in the RC film.

The larger conformational freedom revealed in the absence of trehalose is consistent with recent results of MD simulations and inelastic neutron scattering, performed to compare structural and dynamical properties of glassy matrices formed by the model globular protein lysozyme at low hydration levels in the absence or in the presence of trehalose.[28] Simulations, performed over a hydration range comparable to that of our work, enlighten a number of structural and dynamical

differences between the two matrixes. Among them, the following appear particularly relevant to explain our findings: (i) at a given hydration level, the low frequency part (<50 cm^{-1}) of the vibrational density of states (VDOS) of lysozyme (both simulated and measured by inelastic neutron scattering) is shifted to higher frequencies in the protein-trehalose glass, as compared to the protein alone matrix, suggesting that protein residues experience a stiffer environment in the presence of the sugar; (ii) in the trehalose-protein matrix, the simulated VDOS of water is also shifted to higher frequencies, indicating that water interacts strongly with trehalose; (iii) the mean square displacements obtained from the incoherent neutron scattering spectra (reporting on the motions of hydrogens on the 10 ps timescale), were significantly lower in the trehalose containing matrix, in agreement with the results of simulations performed at 1 ps and 1 ns. Based on the latter finding it was concluded that the presence of trehalose limits the amplitude of both fast and slow protein conformational fluctuations. The different dynamical regimes summarized above have been brought back to differences in the strength, extension, and relaxation of the HB networks which characterize the amorphous protein and protein-trehalose matrices. It is of particular interest that, over a timescale ranging from 10^{-3} to 10^{4} ps, protein-water HBs are found to relax more slowly when trehalose is present in the matrix. This result suggests that, in agreement with the *anchorage* model, the retardation of the protein dynamics by trehalose is to a large extent mediated by the protein hydration layer. The relevance of sub-ps and ps intermolecular collective HB modes in governing the coupling between protein and hydration shell dynamics has been recently supported by THz spectroscopy studies performed in conjunction with MD simulations (for a review see ref. 72).

Water is thought to inject its fast dynamics into the protein, driving specific conformational fluctuations and relaxations on the timescale of biological function (see, e.g. ref. 73). Two classes of solvent controlled protein dynamical processes have been identified:[2] (i) class I, obeying dielectric α relaxations, driven by thermal fluctuation of bulk water, and typically involving large scale internal motions of the protein; (ii) class II, following dielectric β relaxations, coupled to the

hydration shell dynamics, associated with protein rearrangements on a smaller scale. Although the structural bases of the relaxation from the D to the L RC conformations are not fully clarified, the available experimental evidence points to structural alterations on a small scale, like rearrangements of amino acid side chains[56] and/or water molecules weakly bound to the RC.[59] Since the RC relaxation and interconversion between conformational substates are essentially arrested when the hydration shell is removed, according to the unified model of protein dynamics of ref. 2, we have ascribed them to class II, β slaved, processes.[23,44]

When taking into account the notions summarized above, we propose the following scenarios for the dehydration-induced inhibition of RC small scale dynamics in the absence or presence of trehalose. In RC films the retardation of the RC internal motions probed by $P^+Q_A^-$ recombination kinetics is due to the breakdown of the dynamic hydration layer upon dehydration. When the residual water content is reduced below ~10^3 water molecules per RC-detergent complex, the structure and dynamics of the depleted hydration shell are altered,[44] making it unable to inject fast dynamics into the protein-detergent complex[2,73]. Additionally, under these conditions, water-protein and water-detergent HBs are expected to be partially replaced by protein-protein contacts, likely leading to distortions in the overall structure of the RC-detergent complex. Evidence for such distortions has been recently obtained by Raman spectroscopy in the case of lysozyme.[74] Dehydration-induced distortions are possibly in relation with the appearance of a second, much faster (τ~660 μs) component in the $P^+Q_A^-$ recombination kinetics after a laser pulse (section 3.2, and Figure 2). In the dehydrated protein-detergent matrix, the RC retains however the degrees of freedom necessary to completely relax form the dark- to the light-adapted state, when kept for a sufficiently long time in the charge separated state: relaxation is only retarded from the sub-ms to the second timescale, when the hydration shell is depleted.

Also in the case of the RC-trehalose matrix we suggest that RC dynamics is largely governed by that of the hydration layer, which, however, is now more strongly hampered by multiple HBs involving simultaneously residues at the protein surface and trehalose molecules from the matrix.

Direct HBs between trehalose molecules and RC surface groups can further retard the dynamics of the protein. We expect these HB networks result in a tight coupling between the RC- complex and the stiffened trehalose matrix, thus preventing a full relaxation of the RC to the L conformation (section 3.2). The involvement of residual water molecules, H bonded at the protein-matrix interface, in mediating protein-trehalose interactions, evidenced by MD simulations in MbCO,[27] has been recently confirmed by MD simulations in lysozyme,[28] although in this case a larger number of direct trehalose-lysozyme HBs was observed. The scenario proposed above, in line with the *anchorage* hypothesis,[18,29] is also consistent with the parallel inhibition of protein dynamics and relaxation of protein-water HBs, revealed by MD simulations in lysozyme-trehalose glasses.[28]

As an alternative to the *anchorage* hypothesis, the retardation of RC dynamics coupled to $P^+Q_A^-$ stabilization, discussed so far, can be in principle interpreted in terms of β relaxation processes of the whole amorphous system (see Introduction), which are modulated by the hydration level and by the presence of the sugar.[17,46,75,76] In sucrose matrices embedding different proteins, sucrose was found in fact to decrease the amplitude of fast motions, thereby antiplasticizing the β relaxations.[76] A large number of experimental findings indicates that changes in both dynamics and conformational stability of proteins quantitatively track changes in β relaxation dynamics of the entire glassy system.[33] This view does not necessarily imply any protein-matrix *anchorage*. It is our opinion, however, that HB networks are likely to play a role in modulating the RC dynamics, in view of the response of the rate distribution for $P^+Q_A^-$ recombination to prolonged, continuous illumination. As discussed above, not only the average rate constant $\langle k \rangle$ of $P^+Q_A^-$ recombination, but also the width σ of the rate distribution (see Figure 3 and 4, panels B) decreases upon increasing the duration of photoexcitation, clearly indicating that, during continuous illumination, the energy barriers between lower tier conformational substates decrease. This makes possible, on the time scale of charge recombination, the interconversion between conformational substates, which leads to partial averaging (narrowing) of the rate constant distribution. The observed light-induced increase in the lower tier conformational mobility of the RC, which can be easily explained by a

transient disruption of HB networks (see above), does not seem to us simply interpretable without assuming a RC-matrix anchorage.

4.3. The effects of trehalose on slow, large scale RC motions probed by thermal denaturation kinetics.

Small scale protein motions are precursors to denaturation.[33,45-47,49] Since, as discussed in the previous section, small scale RC dynamics, probed by $P^+Q_A^-$ recombination kinetics, are more strongly retarded and restricted in trehalose containing matrices, also the larger scale, slower dynamics associated with the RC thermal denaturation are expected to be correspondingly affected by the presence of trehalose. The RC thermal stability has been the subject of few systematic studies in detergent RC solutions[60,77] and in RC proteoliposomes[61]. A recent analysis in detergent RC solutions[60] has shown that denaturation involves changes in the RC tertiary structure. The non-reversibility of denaturation over the T range examined (from 37°C to 60°C) together with the non-Arrhenius dependence of denaturation rate below a critical temperature (~ 48°C) led the authors to adopt the Lumry and Eyring model[78] as a minimum denaturation scheme, i.e.

$$N \overset{K}{\leftrightarrow} I \overset{k}{\rightarrow} D \qquad (12)$$

in which a non-native conformation I, in equilibrium with the native state N, lies on the pathway from N to the denatured D state. An alternative model (the "offset scheme"), obtained from scheme 12 by exchanging N and I[61], was also considered. Based on the monoexponential character of denaturation kinetics, N and I were assumed in equilibrium on a timescale faster than k^{-1}, so that denaturation was governed by an observable rate constant $k_{app} = kK$ in the case of Lumry and Eyring model, or $k_{app} = k/(1+K)$ for the "offset scheme". Such an assumption appears to hold also in the case of the dehydrated RC film incubated at 44°C, since the decay kinetics of the area of bands 1 and 2, reflecting the release of $BChl_2$ and of monomeric BChls, are reasonably described by a monoexponential function. In view of the above arguments, k_1 and k_2 of scheme 6 (section 3.3)

should be obviously considered as pseudo-first-order rate constant, rather than simple first-order coefficients of a single step, irreversible denaturation.

The decrease of the bands at ~860 nm and ~800 nm clearly indicates that, upon incubation at high temperature, alterations occur in the native environments of $BChl_2$ and monomeric BChl cofactors. However, since these bands are acutely sensitive to the cofactor protein environment, the observed decrease does not necessarily imply, *per se*, that cofactors are released from the binding pockets. At the same time the parallel increase of the spectral components in the 740-770 nm region, besides indicating the release of free BChl and BPheo, might reflect also the loss of the Mg atom by the BChl cofactors. Pheophytinization was excluded by analysis of BChl and BPheo Q_x transitions. Additionally, the Q_x bands of both bacteriochlorin cofactors, as well as of the spheroidenone carotenoid, were found to undergo a progressive blue shift, closely approaching the spectral positions of the RC extracted cofactors in organic solvents. This suggests that bacteriochlorins separate from the protein and mainly interact with the RC-associated detergent micelle. In the case of the dehydrated RC film, the release of the different cofactors occurs in parallel and irreversibly, as judged from the simultaneous decays of the dimeric and monomeric BChl Q_y bands, as well as from the parallel BChl, Bpheo, and carotenoid band shift during denaturation. It is likely, therefore, that the release of the pigments results from a significant disruption of the tertiary structure of the RC complex. RC denaturation kinetics appear therefore to report on the capability of the RC complex to undergo slow, large scale conformational changes in the dehydrated amorphous matrices.

In solution RCs, at 44°C, a rate constant for denaturation $k_{app}=4.9\ 10^{-4}\ s^{-1}$ has been estimated from the decay of the 802 nm band[60]. In dehydrated RC films, decomposition into Gaussian bands, yielded a rate constant $k_{app}=(6.1\pm0.6)\ 10^{-5}\ s^{-1}$ for the decay of the 802 nm band area, indicating that RC dynamics associated with denaturation, is retarded from tens of minutes to a few hours upon dehydration. Thermal stabilization induced by dehydration is well documented by calorimetric investigations in soluble proteins.[47,79,80] The denaturation kinetics observed in RC films show that

depletion of the hydration shell strongly increases thermal stability also in the case of a large membrane protein-detergent complex.

Neutron scattering studies[45,81-84] and MD simulations[28,85] indicated that protein internal motions on the timescale from 10 ps to 1 ns are affected by dehydration in parallel with protein stability, when the residual water content is reduced from 0.2 and 0.1 g of water per g of protein. This has suggested an inverse correlation between thermal stability and protein flexibility, in which the dynamics of the hydration water plays a crucial role.[86] The strong slowing of denaturation kinetics observed by us at low residual hydrations in RC films is consistent with such a suggestion, since it occurs in parallel with the drastic retardation of small scale RC dynamics probed by $P^+Q_A^-$ recombination kinetics following pulsed and continuous photoexcitation.

When the RC is embedded into a dehydrated trehalose glass, at large sugar/protein molar ratios (m=5 10^3), no alteration in the Q_y and Q_x bands of the bacteriochlorin could be detected, even after incubation at 44°C for several days, indicating the suppression of any dynamics associated to thermal denaturation. Such a dramatic stabilization, implying a change of at least 3 orders of magnitude in the rate constant for RC denaturation, prompted us to better define the transition between the dynamical regimes observed in RC films and in RC-trehalose glasses characterized by a sugar content which exceeds, in mass or volume fraction, that of the protein. The evolution of denaturation kinetics upon increasing the molar ratio m reveals that: (i) even a very limited number of trehalose molecule (m=25), interacting with the RC-detergent complex, exerts an antiplasticizing effect on the large scale motions of the complex; (ii) at m close to 500, a transition seems to occur in one or more structural parameters of the protein-sugar matrix, which totally prevents thermal denaturation on the explored time window (4 days); (iii) at $0 < m < 500$, the rate constants for the release of $BChl_2$ and of monomeric BChl cofactors, which coincides in the absence of trehalose (m=0), show a tendency to diverge when m increases, the release of monomeric BChl being generally slower than that of $BChl_2$ (see Table 2).

Point (iii) suggests a different time course in the disruption of the binding pockets of the dimeric and monomeric BChls, possibly related to the sequence of (partial) unfolding of the complex at high temperature. Additionally, at *m*=200, the blue shift of the Q_x band of BPheo is more retarded and reduced in extent than that of BChls (Figure 6A), and no shift is detected in the two carotenoid bands (Figure 6B). It appears that at increasing *m* ratios, the trehalose matrix hampers more effectively the release of the cofactors which are more deeply buried within the protein scaffold (monomeric BChls, BPheos, carotenoid). Upon increasing *m*, also the fractions (f_1 and f_2) of the BChl band areas, which do not decay over the time window examined, tend to increase, suggesting that the dynamics responsible for cofactor release is blocked in an increasing fraction of the RC population.

The behavior summarized in points (i) and (ii) above is consistent with the view that the presence of trehalose results in direct and water-mediated HBs between sugar molecules and the RC complex, as well as between trehalose molecules. When the number of sugar molecules per RC increases, HB networks will develop, extend, and progressively replace protein-protein contacts, giving rise to a progressively tighter structural/dynamical coupling within the RC-trehalose matrix. It can be expected that, at a critical trehalose concentration, the system will undergo a transition, resulting in a dramatic increase of the RC thermal stability. The sequence of events suggested above is based on the structural and dynamical information provided by MD simulations performed in lysozyme alone and lysozyme-trehalose amorphous systems at low hydration levels,[28] already discussed in relation with the retardation of small scale dynamics probed by charge recombination. Besides simulation studies in soluble model proteins,[27,28] experimental studies specifically performed in RC-trehalose and RC-sucrose glasses,[29,43] point to the relevance of interfacial water, and the associated H-bond networks, in governing the dynamics of sugar-embedded proteins. However, as already observed in section 4.2 with reference to the retardation of the fast dynamics associated with $P^+Q_A^-$ stabilization, the drastically increased RC thermal stability conferred by the presence of trehalose within the amorphous dehydrated matrix, as revealed in the present work, can

be in principle connected with the system β relaxation dynamics, without necessarily assuming a role of multiple H-bonds in determining the matrix-protein dynamical coupling. Changes in protein stability have been found to quantitatively correlate with changes in the β relaxation dynamics of different sugar-glass matrices.[33]

Finally we discuss structural parameters which are thought to differ substantially in amorphous protein matrices in the presence or in the absence of trehalose, and which could play an additional role in regulating large scale dynamics and denaturation especially in the case of the RC complex. The comparative MD study by Lerbret and coworkers[28] reveals a free volume fraction f systematically smaller in the presence of trehalose, which embeds amongst lysozyme molecules, considerably improving the molecular packing. The difference between f values in the absence and in the presence of trehalose, increases upon extreme dehydration. Furthermore, the probability distribution functions of the size of the free volume holes differ strikingly in the presence and in the absence of the sugar. In the completely dehydrated systems, the distribution obtained for the lysozyme alone glass is strongly shifted towards large size voids as compared to the one of the lysozyme-trehalose, exhibiting also a peak at ~10^3 $Å^3$, which is not found in the presence of trehalose.

In dehydrated RC films, due to the much larger dimensions (protein M_w~100 KDa) and less regular shape of the RC-detergent complex, as compared to the globular lysozyme (M_w=14.3 KDa), we expect an even worse packing, characterized by larger voids, most of which can be filled by sugar molecules in the RC-trehalose glass. The free volume reduction evidenced by MD simulations in the lysozyme-trehalose glass is in line with experimental estimations of f in protein-sucrose glasses obtained by gas pycnometry.[76] In fact, the free volume fraction f determined in a large fusion protein of human IgG1 (M_w=185 KDa) was found to decrease from 15% in the extensively dehydrated protein alone glass to 5% in a dehydrated sucrose glass with a disaccharide mass fraction equal to 0.8 (corresponding to a sucrose/protein molar ratio of 2164). This experimental result, obtained for a large, irregularly shaped protein, provides a better comparison, when trying to

estimate the free volume in dehydrated RC films. By assuming a mass density of proteins[87] ρ=1.41 g cm^{-3}, a volume V_p=2.2 10^5 $Å^3$ is obtained for the IgG1 protein, and a free volume fraction f =15% corresponds to an average free volume per protein, V_f=3.9 10^4 $Å^3$, accounting for about 18% of the protein volume.

In an attempt to discuss the relevance of these excluded volume effects in the case of RC matrices, particularly in relation with point (ii) above, we make the following assumptions and estimates. The volume of the RC-detergent complex can be roughly evaluated by adopting a geometrical model, as discussed in detail in ref. 44. When including the volume of the oblate ellipsoidal detergent ring,[88] the model yields for the RC-detergent complex a total volume of 3.5 10^5 $Å^3$. To convert trehalose/RC molar ratios, *m*, into average volumes of trehalose per RC complex, we assume an average molecular volume of trehalose, V_T=(369 ± 5) $Å^3$, obtained from the molar volume reported for amorphous trehalose[89]. As a minimum volume we also consider a value V_T=90 $Å^3$, which can be inferred from the distribution of the Voronoi volume for trehalose in MD simulation of a sugar solution at 49% weight fraction.[90] Using the values mentioned above, the critical sugar/RC molar ratio, *m*=500, above which the RC complex becomes thermally stable for days, corresponds to an average trehalose volume per complex ranging between 2 10^5 $Å^3$ and 5 10^4 $Å^3$, depending on the molecular volume assumed for trehalose. This is the same order of magnitude of the free volume per protein, evaluated for the extensively dehydrated IgG1 amorphous matrix in the absence of sugar. We notice that the volume of this protein (V_p=2.2 10^5 $Å^3$) is somewhat smaller than that (3.5 10^5 $Å^3$) of the RC-LDAO complex, which, however, includes a presumably softer detergent belt. Although crude approximations are involved, in view of the order-of-magnitude agreement between the critical trehalose volume and the free volume associated to a dehydrated protein of comparable size, it is tempting to put in relation the filling of voids by the small trehalose molecules, intercalating between protein complexes in the RC-trehalose glass, with the development of the long term stability of the RC complex. It is conceivable that the filling of large voids by trehalose plays a role in determining the total arrest of temperature-induced

alterations in the ternary structure of the RC, introducing an additional structural constraint, and thus contributing to strongly reduce the long term, large scale motional freedom of the complex. The mechanisms discussed above to account for the retardation of the RC dynamics (*anchorage* hypothesis or a role of β relaxation dynamics) do not exclude the concomitant involvement of this structural parameter. MD simulations of lysozyme-trehalose glasses[28] show, in fact, that the improvement of the molecular packing and the formation of an extended and stiffer H-bond network, promoted by the presence of trehalose, are tightly entangled. In the other hypothesis, i.e. when assuming that inhibition of RC dynamics is mainly due to restrictions in the β relaxations of the whole RC-trehalose-water matrix, the connection between free volume and the amplitude of fast β relaxations should be taken into account.[91,92]

5. Conclusions and Outlook

In this work we have determined quantitatively and compared the extent of retardation of protein dynamics induced by dehydration in a large protein complex as the bacterial photosynthetic RC complex when amorphous solid systems are formed in the absence (RC films) or in the presence of the disaccharide trehalose (RC-trehalose glasses). RC dynamics manifested on two different time- and space-scales have been probed, and found to be strongly affected by the presence of trehalose in the glassy matrix, leading to the following main conclusions:

(i) The RC dielectric relaxation associated with the primary charge separation event, involving small scale conformational rearrangements, and occurring in solution on a fast timescale ($\tau < 10^{-3}$ s), is slowed by at least 3 orders of magnitude in the extensively dehydrated matrices. In RC films, the slowed relaxation results in a full stabilization, comparable to that observed in solution, of the primary charged separated state. On the contrary, in the RC-trehalose glass, only a partial stabilization is attained even on tens of seconds, indicating that in the presence of trehalose the conformational energy landscape is much strongly perturbed, being characterized by much

larger energy barriers between conformational states and substates, which more effectively impair RC fluctuations and relaxation.

(ii) Dehydration in the absence of trehalose retards the large scale RC dynamics involved in the release of cofactors during thermal denaturation by one order of magnitude, as compared to solution. These dynamics are further and dramatically slowed by increasing concentrations of trehalose within the matrix. Noteworthy denaturation kinetics is slowed by only 25 trehalose molecules per RC and totally arrested, on the timescale of days, above a threshold of ~500 trehalose molecules per protein complex, suggesting a percolative behaviour. This response to low trehalose concentrations has relevant implications for the use of trehalose amorphous matrices in the long term, room temperature, conservation of labile biomolecules like therapeutic proteins.

(iii) The retardation of thermal RC denaturation in solid trehalose matrices allows to resolve the events associated with loss of the native RC structure, revealing a differential release of cofactors, which is faster and more pronounced for the donor $BChl_2$ dimer, as compared to monomeric, accessory BChls, BPheos, and carotenoids, and does not involve pheophytinization of BChls. This new information can be of interest to improve the thermal stability of hybrid, artificial photosynthetic systems.

(iv) The behavior summarized in point (i) and (ii), i.e. the parallel retardation induced by trehalose in RC dynamics probed by $P^+Q_A^-$ recombination and by thermal denaturation, is fully consistent with the notion that large scale , slow conformational changes, including those leading to loss of the native protein structure,[33,49] are driven by fast, small scale fluctuations.

As a whole results are consistent with the notion that, in amorphous matrices, the structure and dynamics of water-mediated HB at the protein surface play an important role in governing protein dynamics, being deeply perturbed by trehalose. We propose that the effect of trehalose in retarding protein conformational rearrangements on a timescale from 10^{-2} s to 10 s originates from its propensity to form HBs directly with surface groups of the protein-detergent complex and, to a larger extent, with residual water molecules of the protein hydration shell.

As pointed out in sections 4.2 and 4.3, the slowing of RC dynamics induced by the inclusion of trehalose into dehydrated RC amorphous matrices can be in principle explained by the retardation of high frequency β relaxation processes within the whole sugar-RC-water matrix[17,33,46,75,76], without necessarily invoking a prominent role of H-bond networks in the process. A comparative analysis of dielectric relaxation times in RC films and in RC-trehalose glasses, as a function of the trehalose concentration varied over the range explored in the present work, could certainly provide information useful to clarify this point.

Our propensity to consider H-bond interactions as relevant in determining the retardation of RC dynamics was mainly suggested by the observation that, as shown by continuous light experiments, the RC embedded into dried matrices regains its ability to fluctuate between low tier conformational substates when it is maintained for a sufficiently long time in the charge-separated state. Such a property, revealed by the narrowing of the rate distribution for $P^+Q_A^-$ recombination observed under continuous illumination, can be easily accounted for by assuming that the attempts of the RC, kept in the charge separated state, to relax from the dark- to the light-adapted conformation, cause the temporary breakdown of H-bonds involving the RC surface, thus reducing the ruggedness of the RC energy landscape which hampers fluctuations among low tier conformational substates. This light-induced increase of RC conformational mobility seems to us more difficult to explain without invoking an *anchorage* of the RC protein within the amorphous matrix. An *anchorage* model appears also in line with the low number of trehalose molecules per RC complex needed to sizably affect RC thermal denaturation kinetics, and with the percolative transition, at a relatively low sugar/protein molar ratio, which leads to the long term stability. However additional experimental evidences are required to exclude that other mechanisms prevail in determining protein dynamics retardation. We expect that more direct information on the proposed role of trehalose in rearranging and conditioning the structure and dynamics of water-mediated H-bond networks at the protein surface can be obtained by coupling site specific nitroxide-spin labeling of the native RC cysteine at position 156 with high-field EPR

spectroscopy,[93,94] which has been shown to provide information on the proticity of the spin-label environment.[95] Such measurements, comparatively performed in RC-films and in RC-trehalose glasses characterized by different sugar/protein ratio, have been undertaken in the frame of a collaborative project with the Max-Planck-Institute for Chemical Energy Conversion in Mülheim an der Ruhr.

Acknowledgement

The authors thank Klaus Möbius (Free University, Berlin) and Anton Savitsky (Max Planck Institute for Chemical Energy Conversion, Mülheim an der Ruhr) for stimulating, clarifying discussions. Financial support from MIUR of Italy is gratefully acknowledged.

Table 1. Ratio between the areas underlying the Q_x bands of bacteriopheophytin (A_{BPheo}) and of bacteriochlorophyll (A_{BChl}) as a function of the incubation time at 44°C.

Incubation time, t (h)	0	1	2	3	5	7	8
A_{BPheo}/A_{BChl}	0.289	0.284	0.287	0.288	0.286	0.286	0.279

t (h)	23	25	27	29	47	54	117	305
A_{BPheo}/A_{BChl}	0.249	0.245	0.243	0.237	0.236	0.234	0.286	0.243

Table 2. Kinetic parameters of RC denaturation in dehydrated RC films and RC-trehalose matrices characterized by a different sugar/protein molar ratio, *m*. Values of k_1, k_2, f_1, f_2 have been obtained by fitting the area of band 1 and 2 (A_1 and A_2) as a function of the incubation time at 44°C (Figure 9) to eqs.7 and 8. See text for further details.

m	k_1 (h^{-1})	f_1	k_2 (h^{-1})	f_2
0	$(2.5 \pm 0.2)\cdot 10^{-1}$	$(5.0 \pm 1.0)\cdot 10^{-2}$	$(2.0 \pm 0.2)\cdot 10^{-1}$	$(0.8 \pm 0.2)\cdot 10^{-1}$
25	$(1.14 \pm 0.05)\cdot 10^{-1}$	$(1.1 \pm 0.8)\cdot 10^{-2}$	$(4.8 \pm 0.6)\cdot 10^{-2}$	$(0.3 \pm 0.4)\cdot 10^{-1}$
100	$(3.3 \pm 0.4)\cdot 10^{-2}$	$(2.0 \pm 0.2)\cdot 10^{-1}$	$(4.0 \pm 0.7)\cdot 10^{-2}$	$(5.3 \pm 0.2)\cdot 10^{-1}$
200	$(2.2 \pm 0.1)\cdot 10^{-2}$	$(1.9 \pm 0.2)\cdot 10^{-1}$	$(7.0 \pm 3.0)\cdot 10^{-3}$	$(6.0 \pm 0.4)\cdot 10^{-1}$

References

1. Frauenfelder, H.; Sligar, S. G.; Wolynes, P. G. The Energy Landscapes and Motions of Proteins. *Science* **1991,** *254*, 1598-1603.
2. Frauenfelder, H.; Chen, G.; Berendzen, J.; Fenimore, P. W.; Jansson, H.; McMahon, B. H.; Stroe, I. R.; Swenson, J.; Young, R. D. A Unified Model of Protein Dynamics. *Proc. Natl. Acad. Sci. U.S.A.* **2009,** *106*, 5129-5134.
3. Frauenfelder, H.; McMahon, B. Dynamics and Function of Proteins: The Search for General Concepts. *Proc. Natl. Acad. Sci. U.S.A.* **1998,** *95*, 4795-4797.
4. Henzler-Wildman, K.; Kern, D. Dynamic Personalities of Proteins. *Nature* **2007,** *450*, 964-972.
5. Austin, R. H.; Beeson, K. W.; Eisenstein, L.; Frauenfelder, H.; Gunsalus, I. C. Dynamics of Ligand Binding to Myoglobin. *Biochemistry* **1975,** *14*, 5355-5373.
6. McMahon, B. H.; Muller, J. D.; Wraight, C. A.; Nienhaus, G. U. Electron Transfer and Protein Dynamics in the Photosynthetic Reaction Center. *Biophys. J.* **1998,** *74*, 2567-2587.
7. Ansari, A.; Jones, C. M.; Henry, E. R.; Hofrichter, J.; Eaton, W. A. The Role of Solvent Viscosity in the Dynamics of Protein Conformational Changes. *Science* **1992,** *256*, 1796-1798.
8. Helms, V. Protein Dynamics Tightly Connected to the Dynamics of Surrounding and Internal Water Molecules. *ChemPhysChem* **2007,** *8*, 23-33.
9. Rupley, J. A.; Careri, G. Protein Hydration and Function. *Adv. Protein Chem.* **1991,** *41*, 37-172.
10. Prestrelski, S. J.; Tedeschi, N.; Arakawa, T.; Carpenter, J. F. Dehydration-Induced Conformational Transitions in Proteins and Their Inhibition by Stabilizers. *Biophys. J.* **1993,** *65*, 661-671.
11. Crowe, L. M. Lessons from Nature: The Role of Sugars in Anhydrobiosis. *Comp. Biochem. Physiol., Part A: Mol. Integr. Physiol.* **2002,** *131*, 505-513.
12. Albertorio, F.; Chapa, V. A.; Chen, X.; Diaz, A. J.; Cremer, P. S. The α,α-(1→1) Linkage of Trehalose Is Key to Anhydrobiotic Preservation. *J. Am. Chem. Soc.* **2007,** *129*, 10567-10574.

13. Sun, W. Q.; Davidson, P. Protein Inactivation in Amorphous Sucrose and Trehalose Matrices: Effects of Phase Separation and Crystallization. *Biochim. Biophys. Acta, Gen. Subj.* **1998,** *1425*, 235-244.

14. Lopez-Diez, E. C.; Bone, S. The Interaction of Trypsin with Trehalose: An Investigation of Protein Preservation Mechanisms. *Biochim. Biophys. Acta, Gen. Subj.* **2004,** *1673*, 139-148.

15. Choi, H. J.; Yoo, D. G.; Bondy, B. J.; Quan, F. S.; Compans, R. W.; Kang, S. M.; Prausnitz, M. R. Stability of Influenza Vaccine Coated onto Microneedles. *Biomaterials* **2012,** *33*, 3756-3769.

16. Selva, C.; Malferrari, M.; Ballardini, R.; Ventola, A.; Francia, F.; Venturoli, G. Trehalose Preserves the Integrity of Lyophilized Phycoerythrin-Antihuman CD8 Antibody Conjugates and Enhances Their Thermal Stability in Flow Cytometric Assays. *J. Pharm. Sci.* **2013,** *102*, 649-659.

17. Chang, L. Q.; Shepherd, D.; Sun, J.; Ouellette, D.; Grant, K. L.; Tang, X. L.; Pikal, M. J. Mechanism of Protein Stabilization by Sugars During Freeze-Drying and Storage: Native Structure Preservation, Specific Interaction, and/or Immobilization in a Glassy Matrix? *J. Pharm. Sci.* **2005,** *94*, 1427-1444.

18. Cordone, L.; Cottone, G.; Giuffrida, S.; Palazzo, G.; Venturoli, G.; Viappiani, C. Internal Dynamics and Protein-Matrix Coupling in Trehalose-Coated Proteins. *Biochim. Biophys. Acta, Proteins Proteomics* **2005,** *1749*, 252-281.

19. Cordone, L.; Ferrand, M.; Vitrano, E.; Zaccai, G. Harmonic Behavior of Trehalose-Coated Carbon-Monoxy-Myoglobin at High Temperature. *Biophys. J.* **1999,** *76*, 1043-1047.

20. Caliskan, G.; Mechtani, D.; Roh, J. H.; Kisliuk, A.; Sokolov, A. P.; Azzam, S.; Cicerone, M. T.; Lin-Gibson, S.; Peral, I. Protein and Solvent Dynamics: How Strongly Are They Coupled? *J. Chem. Phys.* **2004,** *121*, 1978-1983.

21. Giuffrida, S.; Cottone, G.; Librizzi, F.; Cordone, L. Coupling between the Thermal Evolution of the Heme Pocket and the External Matrix Structure in Trehalose Coated Carboxymyoglobin. *J. Phys. Chem. B* **2003,** *107*, 13211-13217.

22. Cordone, L.; Galajda, P.; Vitrano, E.; Gassmann, A.; Ostermann, A.; Parak, F. A Reduction of Protein Specific Motions in Co-Ligated Myoglobin Embedded in a Trehalose Glass. *Eur. Biophys. J. Biophys. Lett.* **1998,** *27*, 173-176.

23. Savitsky, A.; Malferrari, M.; Francia, F.; Venturoli, G.; Möbius, K. Bacterial Photosynthetic Reaction Centers in Trehalose Glasses: Coupling between Protein Conformational Dynamics and Electron-Transfer Kinetics as Studied by Laser-Flash and High-Field EPR Spectroscopies. *J. Phys. Chem. B* **2010,** *114*, 12729-12743.

24. Hackel, C.; Zinkevich, T.; Belton, P.; Achilles, A.; Reichert, D.; Krushelnitsky, A. The Trehalose Coating Effect on the Internal Protein Dynamics. *Phys. Chem. Chem. Phys.* **2012,** *14*, 2727-2734.

25. Giachini, L.; Francia, F.; Cordone, L.; Boscherini, F.; Venturoli, G. Cytochrome c in a Dry Trehalose Matrix: Structural Dynamical Effects Probed by X-Ray Absorption Spectroscopy. *Biophys. J.* **2007,** *92*, 1350-1360.

26. Cottone, G.; Cordone, L.; Ciccotti, G. Molecular Dynamics Simulation of Carboxy-Myoglobin Embedded in a Trehalose-Water Matrix. *Biophys. J.* **2001,** *80*, 931-938.

27. Cottone, G.; Ciccotti, G.; Cordone, L. Protein-Trehalose-Water Structures in Trehalose Coated Carboxy-Myoglobin. *J. Chem. Phys.* **2002,** *117*, 9862-9866.

28. Lerbret, A.; Affouard, F.; Hedoux, A.; Krenzlin, S.; Siepmann, J.; Bellissent-Funel, M. C.; Descamps, M. How Strongly Does Trehalose Interact with Lysozyme in the Solid State? Insights from Molecular Dynamics Simulation and Inelastic Neutron Scattering. *J. Phys. Chem. B* **2012,** *116*, 11103-11116.

29. Francia, F.; Dezi, M.; Mallardi, A.; Palazzo, G.; Cordone, L.; Venturoli, G. Protein-Matrix Coupling/Uncoupling in "Dry" Systems of Photosynthetic Reaction Center Embedded in

Trehalose/Sucrose: The Origin of Trehalose Peculiarity. *J. Am. Chem. Soc.* **2008,** *130*, 10240-10246.

30. Carpenter, J. F.; Crowe, J. H. An Infrared Spectroscopic Study of the Interactions of Carbohydrates with Dried Proteins. *Biochemistry* **1989,** *28*, 3916-3922.
31. Belton, P. S.; Gil, A. M. IR and Raman-Spectroscopic Studies of the Interaction of Trehalose with Hen Egg-White Lysozyme. *Biopolymers* **1994,** *34*, 957-961.
32. Sampedro, J. G.; Uribe, S. Trehalose-Enzyme Interactions Result in Structure Stabilization and Activity Inhibition. The Role of Viscosity. *Molecular and Cellular Biochemistry* **2004,** *256*, 319-327.
33. Cicerone, M. T.; Douglas, J. F. β-Relaxation Governs Protein Stability in Sugar-Glass Matrices. *Soft Matter* **2012,** *8*, 2983-2991.
34. Palazzo, G.; Mallardi, A.; Hochkoeppler, A.; Cordone, L.; Venturoli, G. Electron Transfer Kinetics in Photosynthetic Reaction Centers Embedded in Trehalose Glasses: Trapping of Conformational Substates at Room Temperature. *Biophys. J.* **2002,** *82*, 558-568.
35. Francia, F.; Palazzo, G.; Mallardi, A.; Cordone, L.; Venturoli, G. Residual Water Modulates Q_A^--to-Q_B Electron Transfer in Bacterial Reaction Centers Embedded in Trehalose Amorphous Matrices. *Biophys. J.* **2003,** *85*, 2760-2775.
36. Francia, F.; Palazzo, G.; Mallardi, A.; Cordone, L.; Venturoli, G. Probing Light-Induced Conformational Transitions in Bacterial Photosynthetic Reaction Centers Embedded in Trehalose-Water Amorphous Matrices. *Biochim. Biophys. Acta, Bioenerg.* **2004,** *1658*, 50-57.
37. Feher, G.; Allen, J. P.; Okamura, M. Y.; Rees, D. C. Structure and Function of Bacterial Photosynthetic Reaction Centers. *Nature* **1989,** *339*, 111-116.
38. McElroy, J. D.; Mauzerall, D. C.; Feher, G. Characterization of Primary Reactants in Bacterial Photosynthesis. II. Kinetic Studies of the Light-Induced EPR Signal (g = 2.0026) and the Optical Absorbance Changes at Cryogenic Temperatures. *Biochim. Biophys. Acta* **1974,** *333*, 261-278.

39. Wang, H.; Lin, S.; Allen, J. P.; Williams, J. C.; Blankert, S.; Laser, C.; Woodbury, N. W. Protein Dynamics Control the Kinetics of Initial Electron Transfer in Photosynthesis. *Science* **2007,** *316*, 747-750.

40. Graige, M. S.; Feher, G.; Okamura, M. Y. Conformational Gating of the Electron Transfer Reaction $Q_A^{-\cdot}Q_B \rightarrow Q_AQ_B^{-\cdot}$ in Bacterial Reaction Centers of *Rhodobacter Sphaeroides* Determined by a Driving Force Assay. *Proc. Natl. Acad. Sci. U.S.A.* **1998,** *95*, 11679-11684.

41. Kleinfeld, D.; Okamura, M. Y.; Feher, G. Electron-Transfer Kinetics in Photosynthetic Reaction Centers Cooled to Cryogenic Temperatures in the Charge-Separated State: Evidence for Light-Induced Structural Changes. *Biochemistry* **1984,** *23*, 5780-5786.

42. Kriegl, J. M.; Forster, F. K.; Nienhaus, G. U. Charge Recombination and Protein Dynamics in Bacterial Photosynthetic Reaction Centers Entrapped in a Sol-Gel Matrix. *Biophys. J.* **2003,** *85*, 1851-1870.

43. Francia, F.; Malferrari, M.; Sacquin-Mora, S.; Venturoli, G. Charge Recombination Kinetics and Protein Dynamics in Wild Type and Carotenoid-Less Bacterial Reaction Centers: Studies in Trehalose Glasses. *J. Phys. Chem. B* **2009,** *113*, 10389-10398.

44. Malferrari, M.; Francia, F.; Venturoli, G. Coupling between Electron Transfer and Protein-Solvent Dynamics: FTIR and Laser-Flash Spectroscopy Studies in Photosynthetic Reaction Center Films at Different Hydration Levels. *J. Phys. Chem. B* **2011,** *115*, 14732-14750.

45. Tsai, A. M.; Udovic, T. J.; Neumann, D. A. The Inverse Relationship between Protein Dynamics and Thermal Stability. *Biophys. J.* **2001,** *81*, 2339-2343.

46. Cicerone, M. T.; Soles, C. L. Fast Dynamics and Stabilization of Proteins: Binary Glasses of Trehalose and Glycerol. *Biophys. J.* **2004,** *86*, 3836-3845.

47. Cinelli, S.; De Francesco, A.; Onori, G.; Paciaroni, A. Thermal Stability and Internal Dynamics of Lysozyme as Affected by Hydration. *Phys. Chem. Chem. Phys.* **2004,** *6*, 3591-3595.

48. Fenimore, P. W.; Frauenfelder, H.; McMahon, B. H.; Young, R. D. Bulk-Solvent and Hydration-Shell Fluctuations, Similar to α- and β-Fluctuations in Glasses, Control Protein Motions and Functions. *Proc. Natl. Acad. Sci. U.S.A.* **2004,** *101*, 14408-14413.

49. Frauenfelder, H.; Fenimore, P. W.; Chen, G.; McMahon, B. H. Protein Folding Is Slaved to Solvent Motions. *Proc. Natl. Acad. Sci. U.S.A.* **2006,** *103*, 15469-15472.

50. Baciou, L.; Michel, H. Interruption of the Water Chain in the Reaction Center from *Rhodobacter Sphaeroides* Reduces the Rates of the Proton Uptake and of the Second Electron Transfer to Q_B. *Biochemistry* **1995,** *34*, 7967-7972.

51. Giustini, M.; Palazzo, G.; Colafemmina, G.; DellaMonica, M.; Giomini, M.; Ceglie, A. Microstructure and Dynamics of the Water-in-Oil CTAB/n-Pentanol/n-Hexane/Water Microemulsion: A Spectroscopic and Conductivity Study. *J. Phys. Chem.* **1996,** *100*, 3190-3198.

52. Bevington, P. R., *Data Reduction and Error Analysis for the Physical Sciences*. McGraw-Hill: New York, 1969.

53. Chan, R. H.; Bogomolni, R. A. Structural Water Cluster as a Possible Proton Acceptor in the Adduct Decay Reaction of Oat Phototropin 1 LOV2 Domain. *J. Phys. Chem. B* **2012,** *116*, 10609-10616.

54. Ortega, J. M.; Mathis, P.; Williams, J. C.; Allen, J. P. Temperature Dependence of the Reorganization Energy for Charge Recombination in the Reaction Center from *Rhodobacter Sphaeroides*. *Biochemistry* **1996,** *35*, 3354-3361.

55. Kriegl, J. M.; Nienhaus, G. U. Structural, Dynamic, and Energetic Aspects of Long-Range Electron Transfer in Photosynthetic Reaction Centers. *Proc. Natl. Acad. Sci. U.S.A.* **2004,** *101*, 123-128.

56. Nabedryk, E.; Bagley, K. A.; Thibodeau, D. L.; Bauscher, M.; Mäntele, W.; Breton, J. A Protein Conformational Change Associated with the Photoreduction of the Primary and Secondary Quinones in the Bacterial Reaction Center. *FEBS Lett.* **1990,** *266*, 59-62

57. Wöhri, A. B.; Katona, G.; Johansson, L. C.; Fritz, E.; Malmerberg, E.; Andersson, M.; Vincent, J.; Eklund, M.; Cammarata, M.; Wulff, M.; Davidsson, J.; Groenhof, G.; Neutze, R. Light-Induced Structural Changes in a Photosynthetic Reaction Center Caught by Laue Diffraction. *Science* **2010,** *328*, 630-633.

58. Malferrari, M.; Mezzetti, A.; Francia, F.; Venturoli, G. Effects of Dehydration on Light-Induced Conformational Changes in Bacterial Photosynthetic Reaction Centers Probed by Optical and Differential FTIR Spectroscopy. *Biochim. Biophys. Acta, Bioenerg.* **2013,** *1827*, 328-339.

59. Iwata, T.; Paddock, M. L.; Okamura, M. Y.; Kandori, H. Identification of FTIR Bands Due to Internal Water Molecules around the Quinone Binding Sites in the Reaction Center from *Rhodobacter Sphaeroides*. *Biochemistry* **2009,** *48*, 1220-1229.

60. Palazzo, G.; Lopez, F.; Mallardi, A. Effect of Detergent Concentration on the Thermal Stability of a Membrane Protein: The Case Study of Bacterial Reaction Center Solubilized by N,N-Dimethyldodecylamine-N-Oxide. *Biochim. Biophys. Acta, Proteins Proteomics* **2010,** *1804*, 137-146.

61. Hughes, A. V.; Rees, P.; Heathcote, P.; Jones, M. R. Kinetic Analysis of the Thermal Stability of the Photosynthetic Reaction Center from *Rhodobacter Sphaeroides*. *Biophys. J.* **2006,** *90*, 4155-4166.

62. Reed, D. W.; Peters, G. A. Characterization of the Pigments in Reaction Center Preparations from *Rhodopseudomonas Spheroides*. *J. Biol. Chem.* **1972,** *247*, 7148-7152.

63. Beugeling, T.; Slooten, L.; Barelds-Van de Beek, P. G. M. N. Thin-Layer Chromatography of Pigments from Reaction Center Particles of *Rhodopseudomonas Sphaeroides*. *Biochim. Biophys. Acta, Bioenerg.* **1972,** *283*, 328-333.

64. Van der Rest, M.; Gingras, G. The Pigment Complement of the Photosynthetic Reaction Center Isolated from *Rhodospirillum Rubrum*. *J. Biol. Chem.* **1974,** *249*, 6446-6453.

65. Malferrari, M.; Nalepa, A.; Venturoli, G.; Francia, F.; Lubitz, W.; Möbius, K.; Savitsky, A. Structural and Dynamical Characteristics of Trehalose and Sucrose Matrices at Different Hydration Levels as Probed by FTIR and High-Field EPR. *Phys. Chem. Chem. Phys.* **2014,** *16*, 9831-9848.

66. Douglas, J. F.; Johnson, H. E.; Granick, S. A Simple Kinetic-Model of Polymer Adsorption and Desorption. *Science* **1993,** *262*, 2010-2012.

67. McCutcheon, A. L.; Barton, W. A.; Wilson, M. A. Kinetics of Water Adsorption/Desorption on Bituminous Coals. *Energy Fuels* **2001,** *15*, 1387-1395.

68. Marabi, A.; Livings, S.; Jacobson, M.; Saguy, I. S. Normalized Weibull Distribution for Modeling Rehydration of Food Particulates. *Eur. Food Res. Technol.* **2003,** *217*, 311-318.

69. Garcia-Pascual, P.; Sanjuan, N.; Melis, R.; Mulet, A. *Morchella Esculenta* (morel) Rehydration Process Modelling. *J. Food Eng.* **2006,** *72*, 346-353.

70. Xie, G. F.; Timasheff, S. N. The Thermodynamic Mechanism of Protein Stabilization by Trehalose. *Biophys. Chem.* **1997,** *64*, 25-43.

71. Timasheff, S. N. Protein Hydration, Thermodynamic Binding, and Preferential Hydration. *Biochemistry* **2002,** *41*, 13473-13482.

72. Conti Nibali, V.; Havenith, M. New Insights into the Role of Water in Biological Function: Studying Solvated Biomolecules Using Terahertz Absorption Spectroscopy in Conjunction with Molecular Dynamics Simulations. *J. Am. Chem. Soc.* **2014,** *136*, 12800-12807.

73. Bizzarri, A. R.; Cannistraro, S. Molecular Dynamics of Water at the Protein-Solvent Interface. *J. Phys. Chem. B* **2002,** *106*, 6617-6633.

74. Kocherbitov, V.; Latynis, J.; Misiunas, A.; Barauskas, J.; Niaura, G. Hydration of Lysozyme Studied by Raman Spectroscopy. *J. Phys. Chem. B* **2013,** *117*, 4981-4992.

75. Yoshioka, S.; Miyazaki, T.; Aso, Y. β-Relaxation of Insulin Molecule in Lyophilized Formulations Containing Trehalose or Dextran as a Determinant of Chemical Reactivity. *Pharm. Res.* **2006,** *23*, 961-966.

76. Wang, B.; Tchessalov, S.; Cicerone, M. T.; Warne, N. W.; Pikal, M. J. Impact of Sucrose Level on Storage Stability of Proteins in Freeze-Dried Solids: II. Correlation of Aggregation Rate with Protein Structure and Molecular Mobility. *J. Pharm. Sci.* **2009,** *98*, 3145-3166.

77. Tandori, J.; Tokaji, Z.; Misurda, K.; Maroti, P. Thermodynamics of Light-Induced and Thermal Degradation of Bacteriochlorins in Reaction Center Protein of Photosynthetic Bacteria. *Photochem. Photobiol.* **2005,** *81*, 1518-1525.

78. Lumry, F.; Eyring, H. Conformation Change of Proteins. *J. Phys. Chem.* **1954,** *58*, 110-120.

79. Bell, L. N.; Hageman, M. J.; Bauer, J. M. Impact of Moisture on Thermally-Induced Denaturation and Decomposition of Lyophilized Bovine Somatotropin. *Biopolymers* **1995,** *35*, 201-209.

80. Bell, L. N.; Hageman, M. J.; Muraoka, L. M. Thermally-Induced Denaturation of Lyophilized Bovine Somatotropin and Lysozyme as Impacted by Moisture and Excipients. *J. Pharm. Sci.* **1995,** *84*, 707-712.

81. Tsai, A. M.; Neumann, D. A.; Bell, L. N. Molecular Dynamics of Solid-State Lysozyme as Affected by Glycerol and Water: A Neutron Scattering Study. *Biophys. J.* **2000,** *79*, 2728-2732.

82. Sokolov, A. P.; Roh, J. H.; Mamontov, E.; Sakai, V. G. Role of Hydration Water in Dynamics of Biological Macromolecules. *Chem. Phys.* **2008,** *345*, 212-218.

83. Paciaroni, A.; Cinelli, S.; Onori, G. Effect of the Environment on the Protein Dynamical Transition: A Neutron Scattering Study. *Biophys. J.* **2002,** *83*, 1157-1164.

84. Paciaroni, A.; Orecchini, A.; Cinelli, S.; Onori, G.; Lechner, R. E.; Pieper, J. Protein Dynamics on the Picosecond Timescale as Affected by the Environment: A Quasielastic Neutron Scattering Study. *Chem. Phys.* **2003,** *292*, 397-404.

85. Roh, J. H.; Curtis, J. E.; Azzam, S.; Novikov, V. N.; Peral, I.; Chowdhuri, Z.; Gregory, R. B.; Sokolov, A. P. Influence of Hydration on the Dynamics of Lysozyme. *Biophys. J.* **2006,** *91*, 2573-2588.

86. Young, R. D.; Fenimore, P. W. Coupling of Protein and Environment Fluctuations. *Biochim. Biophys. Acta, Proteins Proteomics* **2011,** *1814*, 916-921.

87. Fischer, H.; Polikarpov, I.; Craievich, A. F. Average Protein Density Is a Molecular-Weight-Dependent Function. *Protein Sci.* **2004,** *13*, 2825-2828.

88. Le Maire, M.; Kwee, S.; Andersen, J. P.; Moller, J. V. Mode of Interaction of Polyoxyethyleneglycol Detergents with Membrane Proteins. *Eur. J. Biochem.* **1983,** *129*, 525-532.

89. Miller, D. P.; dePablo, J. J.; Corti, H. Thermophysical Properties of Trehalose and Its Concentrated Aqueous Solutions. *Pharm. Res.* **1997,** *14*, 578-590.

90. Bordat, P.; Lerbret, A.; Demaret, J. P.; Affouard, F.; Descamps, M. Comparative Study of Trehalose, Sucrose and Maltose in Water Solutions by Molecular Modelling. *Europhys. Lett.* **2004,** *65*, 41-47.

91. Ngai, K. L.; Bao, L. R.; Yee, A. F.; Soles, C. L. Correlation of Positron Annihilation and Other Dynamic Properties in Small Molecule Glass-Forming Substances. *Phys. Rev. Lett.* **2001,** *87, 215901*.

92. Starr, F. W.; Sastry, S.; Douglas, J. F.; Glotzer, S. C. What Do We Learn from the Local Geometry of Glass-Forming Liquids? *Phys. Rev. Lett.* **2002,** *89, 125501*.

93. Poluektov, O. G.; Utschig, L. M.; Dalosto, S.; Thurnauer, M. C. Probing Local Dynamics of the Photosynthetic Bacterial Reaction Center with a Cysteine Specific Spin Label. *J. Phys. Chem. B* **2003,** *107*, 6239-6244.

94. Borovykh, I. V.; Ceola, S.; Gajula, P.; Gast, P.; Steinhoff, H. J.; Huber, M. Distance between a Native Cofactor and a Spin Label in the Reaction Centre of *Rhodobacter Sphaeroides* by a Two-Frequency Pulsed Electron Paramagnetic Resonance Method and Molecular Dynamics Simulations. *J. Magn. Res.* **2006,** *180*, 178-185.

95. Plato, M.; Steinhoff, H. J.; Wegener, C.; Torring, J. T.; Savitsky, A.; Möbius, K. Molecular Orbital Study of Polarity and Hydrogen Bonding Effects on the g and Hyperfine Tensors of Site Directed NO Spin Labelled Bacteriorhodopsin. *Mol. Phys.* **2002,** *100*, 3711-3721.

Figure captions.

Figure 1.

Dehydration/rehydration kinetics of RC-trehalose matrices, characterized by a trehalose/RC molar ratio equal to 5 10^3, equilibrated at different relative humidities. Panel A shows the sequence of two dehydration phases (at r=11% and r=3%) and a subsequent rehydration (from r=3% to r=11%). The initial dehydration kinetics is enlarged in panel B. Different symbols correspond to different RC-trehalose glasses. Black and red lines are best fit to exponential and to stretched exponential kinetics, respectively (see Discussion, eqs.10-11). Best fitting parameters are: τ=14.6 h (exponential), τ=9.8 h and β=0.42 (stretched exponential) for dehydration at r=11%; τ=48.0 h (exponential), τ=63.0 h and β=0.55 (stretched exponential) for dehydration at r=3%; τ=29.1 h (exponential), τ=28.0 h and β=0.77 (stretched exponential) for rehydration at r=11%. According to the stretched exponential fit, the content of residual water corresponds to a molar ratio (H_2O/trehalose)=0.47±0.03 following the first equilibration at r=11%, to (H_2O/trehalose)=0.04±0.02 upon equilibration at r=3%, and to (H_2O/trehalose)=0.42±0.03 when the sample is re-incubated at r=11%.

Figure 2.

The effect of continuous illumination on $P^+Q_A^-$ recombination kinetics in a RC-trehalose matrix (A) and in a RC film (B), equilibrated at the same relative humidity, r=11%. The RC-trehalose matrix was characterized by a sugar/RC molar ratio equal to 5 10^3. In the RC-trehalose glass, residual water corresponds to a molar ratio (H_2O/trehalose)=0.48, i.e. (H_2O/RC)=2.4 10^3. In the RC film a value of 900 water molecules per RC has been determined. Kinetic traces recorded after a laser pulse and after a period Δt=20 s of continuous illumination are shown in black and green, respectively. Both panels also show, for the sake of comparison, the kinetics recorded after a laser pulse (blue traces) in a liquid RC suspension (3 μM RC in 10 mM Tris buffer, pH 8.0, 10 mM o-phenanthroline, 0.025 % LDAO). The time t=0 corresponds to the laser pulse or to the closure of

the shutter gating the continuous photoexcitation. Traces have been normalized to the respective amplitudes at t=0. Red curves represent best fitting to a single power law (eq. 1), except for the trace recorded in the RC film after the laser pulse, which included an additional, faster kinetic component, also fitted to a power law decay. Best fitting kinetic parameters are reported in the text. The insets show the corresponding rate distribution functions *f(k)* defined on a logarithmic scale [$p(k)dk = f(k)\, d\, log(k)$], calculated according to eq.3.

Figure 3.

Dependence of the kinetic parameters of $P^+Q_A^-$ recombination upon the duration Δt of continuous illumination in RC-trehalose matrices (open squares) and in RC films (filled circles) equilibrated at r=11%. Kinetics have been analyzed as illustrated in Fig. 2. Values of the average rate constant, $\langle k \rangle$, and of the rate distribution width, σ, are shown in panel (A) and (B), respectively. Vertical bars indicate confidence intervals within two standard deviations. For the sake of comparison, $\langle k \rangle$ and σ values determined in solution RCs are also shown (open diamonds). For the latter values, the errors are smaller than the symbol size.

Figure 4.

The average rate constant, $\langle k \rangle$ (panel A), and the rate distribution width, σ (panel B), as a function of the duration Δt of illumination, obtained by analyzing the kinetics of $P^+Q_A^-$ recombination in RC-trehalose matrices (open squares) and in RC films (filled circles) equilibrated at r=3%. Vertical bars indicate confidence intervals within two standard deviations. The RC-trehalose glass was characterized by a molar ratio (H_2O/trehalose)=4 10^{-2}. In the RC film the content of residual water corresponds to ~ 80 water molecules per RC. Values of $\langle k \rangle$ and σ determined in solution RCs are shown as open diamonds.

Figure 5.

A. Near-infrared absorbance spectra of a dehydrated RC-trehalose matrix, characterized by a sugar/RC molar ratio m=5 10^3, recorded before (t=0 h) and after a prolonged (t=96 h) exposure to 44°C. Spectra have been offset for clarity. Decomposition into four Gaussian bands, centered at 858 nm, 803 nm, 757 nm, and 700 nm, is shown for the lower spectrum (t=96 h). **B-D.** Time evolution of the NIR spectrum of a RC film, recorded at selected times t during incubation at 44°C. Except for the spectrum measured before incubation (panel B, t=0 h), decomposition of the spectra included, besides the 4 bands arising from the bound bacteriochlorin RC cofactors, 2 additional Gaussian bands, centered at 770 nm (band 5) and 750 nm (band 6), corresponding to the spectral contributions of BChls and BPheos released by the RC during denaturation (panels C and D). Thick continuous lines represent the resulting best fit (see text for the details of the fitting procedure). The individual Gaussian bands are shown with thin lines for each spectrum.

Figure 6.

The Q_x region of absorbance spectra recorded in a RC film before (black line) and after incubation at 44°C for 7 hours (red line). Labels mark the peak positions of the BChl and BPheo bands (597 nm and 534 nm, respectively, at t=0) and of two bands (505 nm and 471 nm, at t=0 h) of the RC carotenoid spheroidenone.

Figure 7.

The peak wavelength of the BChl and BPheo Q_x bands (panel A), and of two bands of the RC carotenoid spheroidenone (panel B) as a function of the incubation time at 44°C in RC films (black symbols) and in RC trehalose glasses characterized by two sugar/RC molar ratios, m (red symbols, m=25; green symbols, m=200). Due to the increasing light scattering, the peak position of the carotenoid bands, centered at 505 nm and 471 nm at t=0 h, could not be determined with an acceptable confidence for long periods of incubation at high temperature in the RC films and in RC

trehalose glasses at m=25. Light scattering also prevented to study the shift of the third carotenoid band, peaking at a shorter wavelength (~ 445 nm at t= 0 h, see Figure 6).

Figure 8.

The kinetics of RC denaturation at 44°C in a dehydrated RC film. NIR spectra have been decomposed into 6 Gaussian bands as illustrated in Figure 5 C, D. Panels **A** and **B** show the dependence upon the incubation time of the areas A_1 and A_2 of the bands ascribed to $BChl_2$ and to the monomeric BChls bound to the RC. The corresponding time evolution of the area A_5 of the band at 770 nm (attributed to the released BChls) is presented in panel **C**. Vertical bars give confidence intervals within 2 standard deviations. Continuous lines represent the best fitting of $A_1(t)$, $A_2(t)$ *and* $A_5(t)$ to eqs. 7-9 (see text for further details). The values of the best fitting parameters are: $A_1(0)$= (9.3 ± 0.3) nm, k_1=(2.5 ± 0.2) 10^{-1} h^{-1}, f_1=(5 ± 1) 10^{-2}, $A_2(0)$=(9.7 ± 0.5) nm, k_2=(2.2 ± 0.2) 10^{-1} h^{-1}, f_2=(0.8 ± 0.2) 10^{-1}, A'_5=(9.0 ± 0.5) nm. .

Figure 9.

The effect of the trehalose/protein molar ratio, m, on the kinetics of RC denaturation at 44°C in dehydrated RC-trehalose matrices. Data (symbols and continuous lines) are plotted using the following color code: black, m=0; red, m=25, blue, m=100; green, m=200; orange, m=500; magenta, m=10^3; purple, m=10^4. Panels **A** and **B** show the areas $A_1(t)$ and $A_2(t)$ as a function of the incubation time t. The corresponding increase of the area $A_5(t)$ of the band at 770 nm (ascribed to the released BChls) is reported in panel **C**. For $0 < m \leq 200$ the NIR spectra acquired during incubation have been decomposed into 6 Gaussian bands, as illustrated in Figure 5 (panel C and D) for the RC film (m=0). In samples characterized by $m > 200$ the NIR spectra were not significantly affected by exposure to high temperature, and were fitted to the sum of the 4 Gaussian bands corresponding to the contribution of RC bound cofactors. For these m values (500, 10^3, 10^4), therefore, only the time evolution of the areas of band 1 and 2 is reported in panels A and B, being the area of the band ascribed to free BChls set to zero. Continuous lines (for data sets corresponding to $0 < m \leq 200$)

represent the fitting of $A_1(t)$, $A_2(t)$, $A_5(t)$ to eqs.7-9 (see text for further details). Best fitting parameters are reported in Table 2.

Figure 10.

Schematic representation of the rugged free energy surfaces of the neutral, PQ_A, and charge separated state ($P^+Q_A^-$) of the RC, as a function of the conformational coordinate q. D (q=0) and L (q=1) correspond to the dark- and light-adapted conformation. Red and blue arrows depict charge separation and recombination processes, respectively. The latter include relaxation from the D towards the L conformation by diffusive motions on the $P^+Q_A^-$ surface. The kinetics of charge recombination is determined by the free energy gap E(q). Figure adapted from ref. 55.

Figure 1

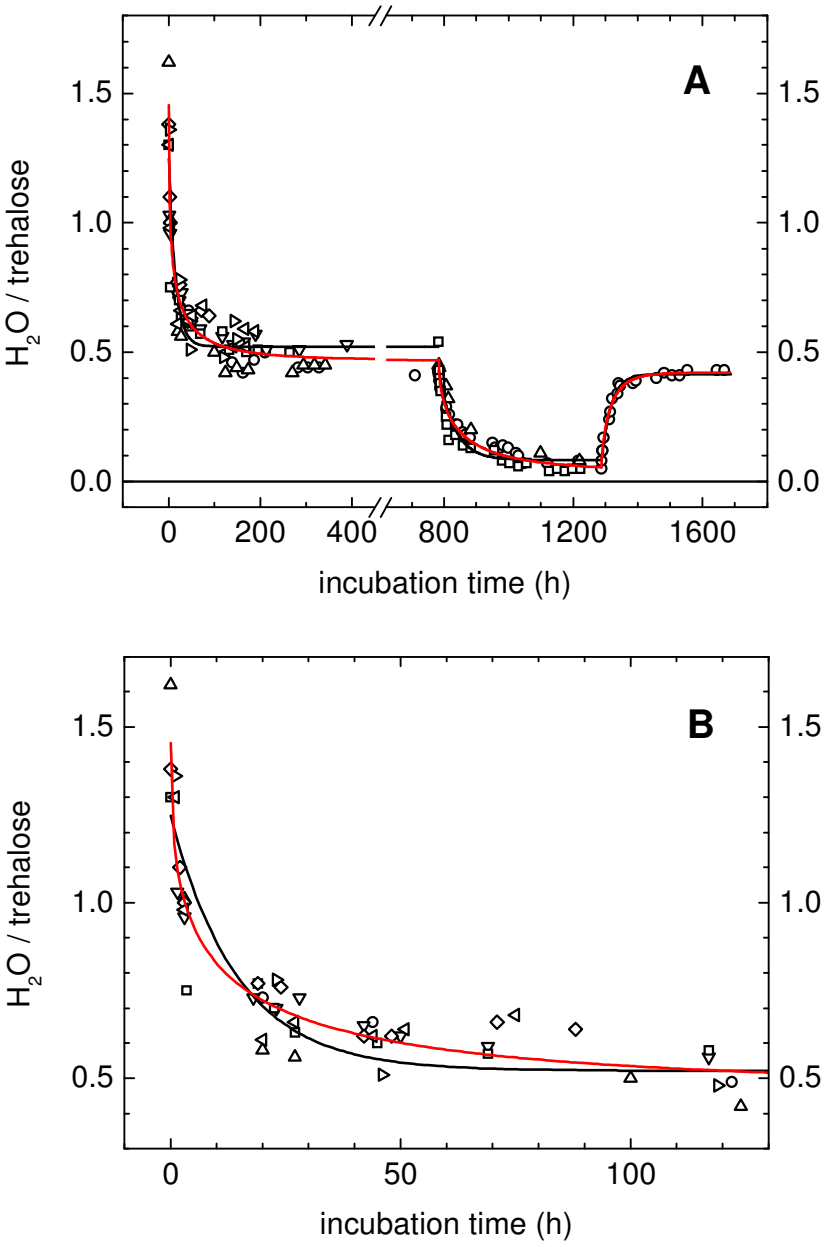
A
B
H_2O / trehalose
incubation time (h)
0.0
0.5
1.0
1.5
0
200
400
800
1200
1600
50
100

Figure 2

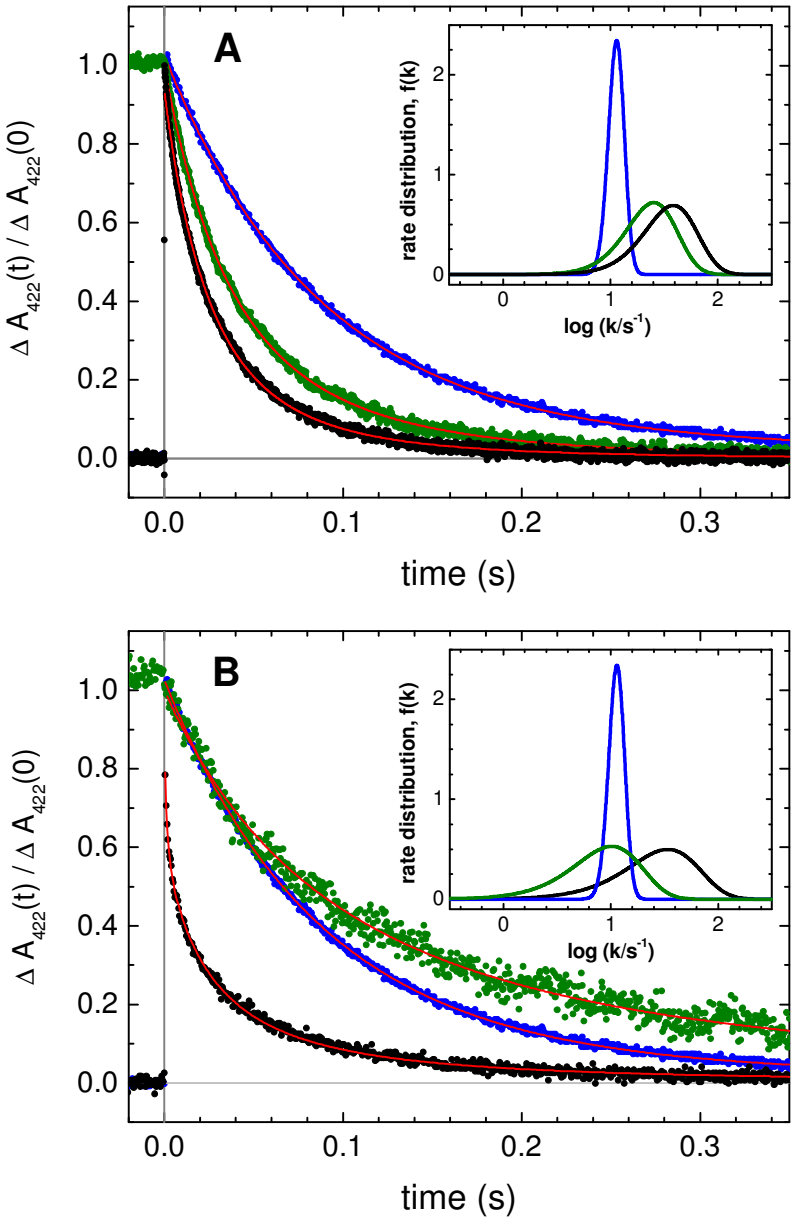
A
B
Δ A422(t) / Δ A422(0)
time (s)
rate distribution, f(k)
log (k/s-1)
0.0
0.2
0.4
0.6
0.8
1.0
0.1
0.3
0
1
2

Figure 3

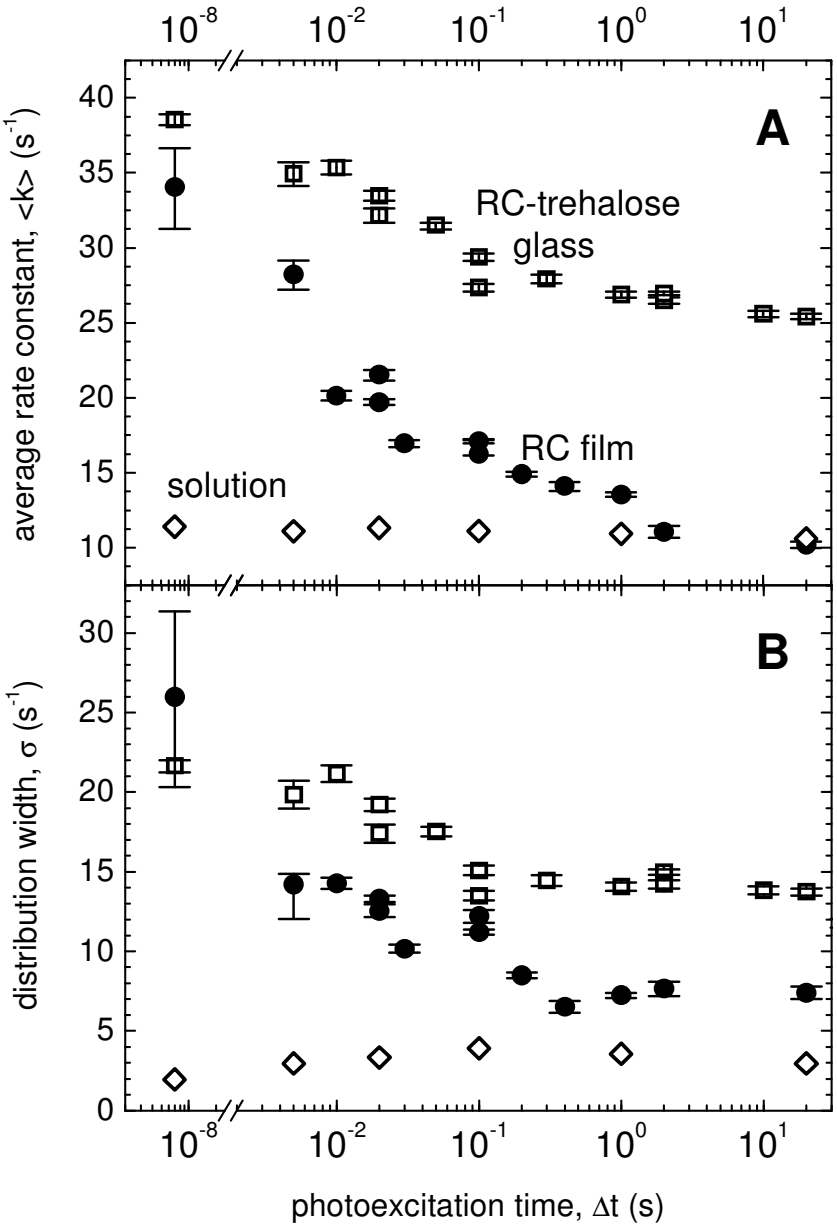
A
B
RC-trehalose glass
RC film
solution
average rate constant, <k> (s-1)
distribution width, σ (s-1)
photoexcitation time, Δt (s)

Figure 4

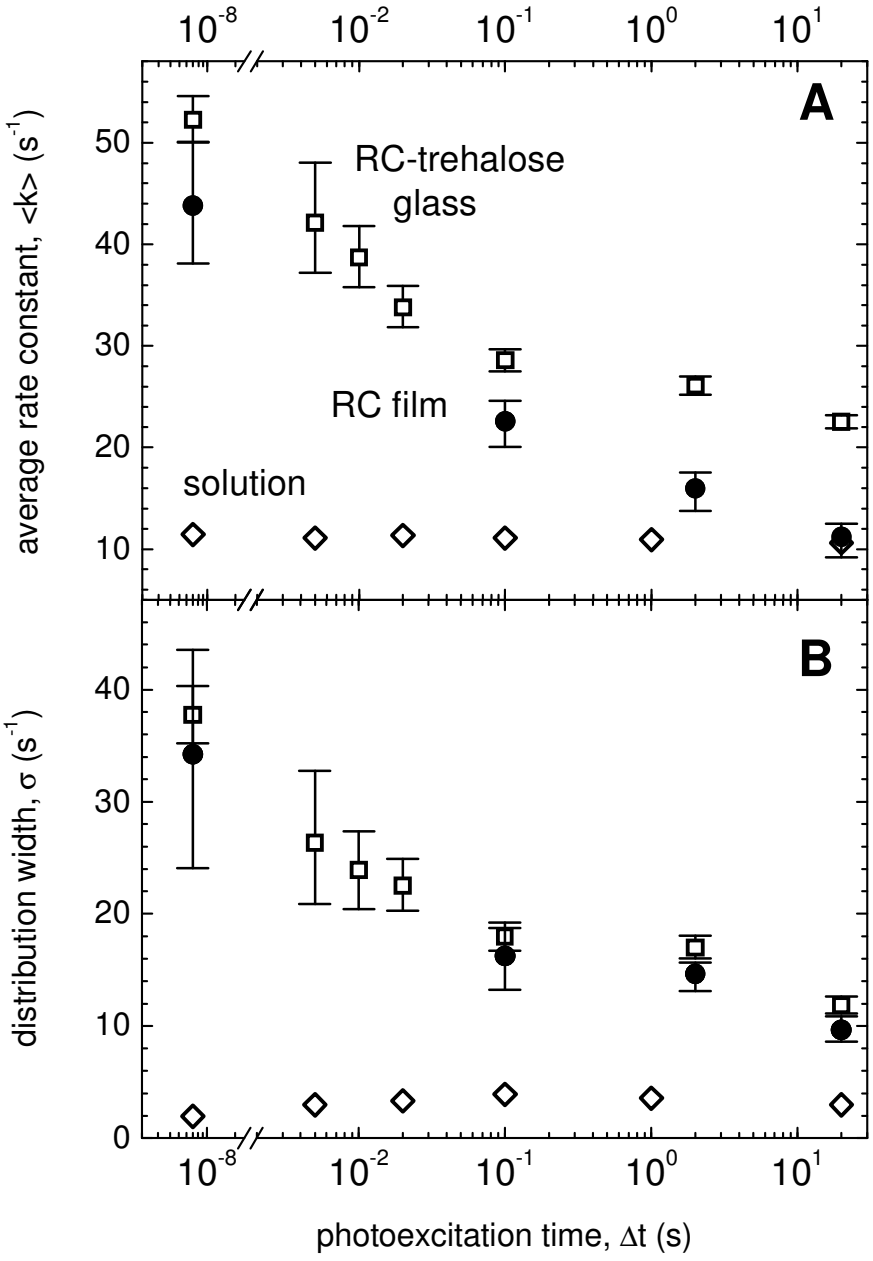
A
B
RC-trehalose glass
RC film
solution
average rate constant, <k> (s-1)
distribution width, σ (s-1)
photoexcitation time, Δt (s)
10-8
10-2
10-1
100
101
0
10
20
30
40
50

Figure 5

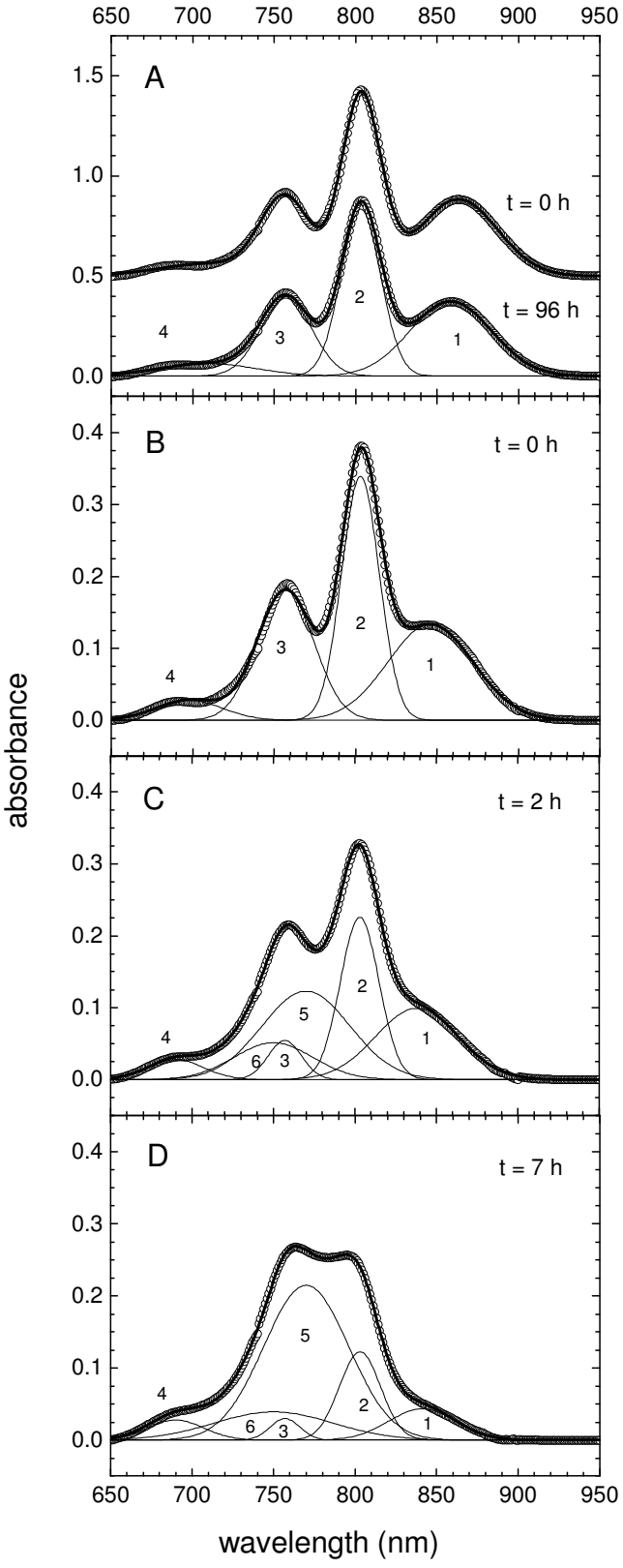

Figure 6

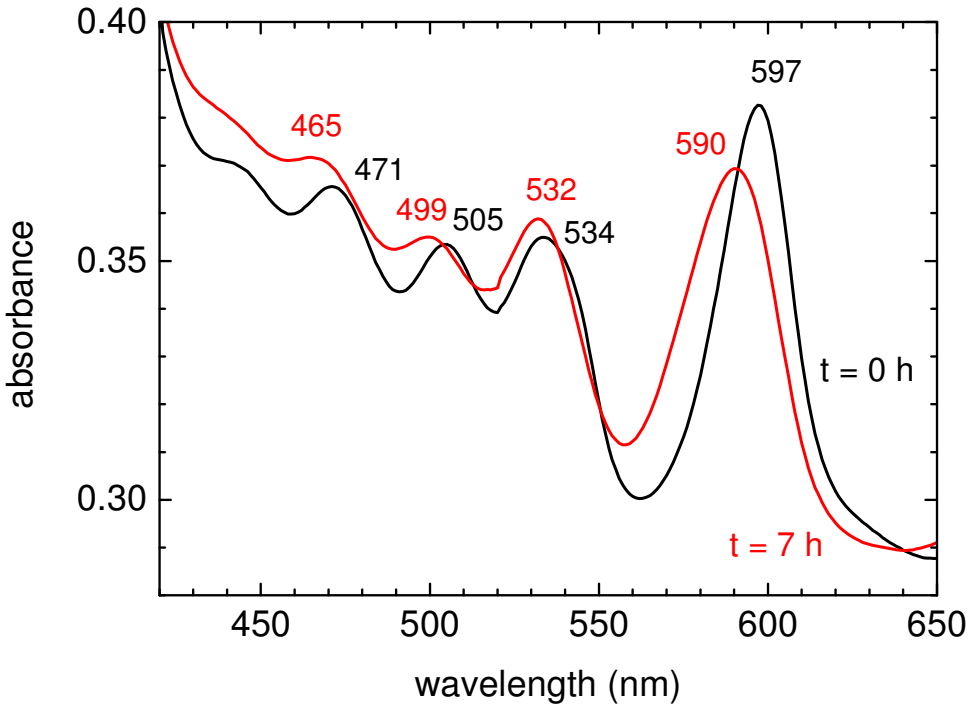
0.40
0.35
0.30
absorbance
450
500
550
600
650
wavelength (nm)
465
471
499
505
532
534
590
597
t = 0 h
t = 7 h

Figure 7

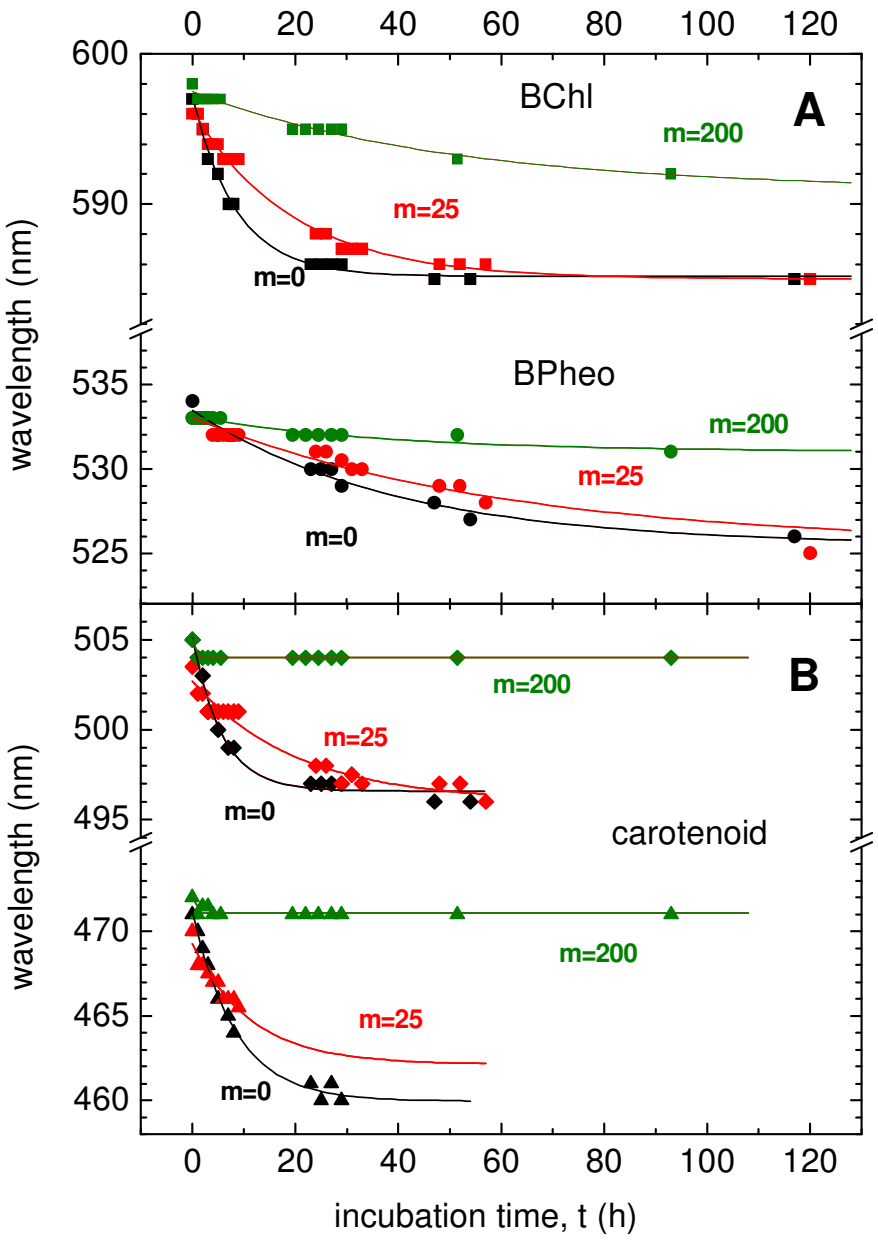
BChl
A
m=200
m=25
m=0
BPheo
m=200
m=25
m=0
B
m=200
m=25
m=0
carotenoid
m=200
m=25
m=0
wavelength (nm)
wavelength (nm)
incubation time, t (h)
0
20
40
60
80
100
120
600
590
535
530
525
505
500
495
470
465
460

Figure 8

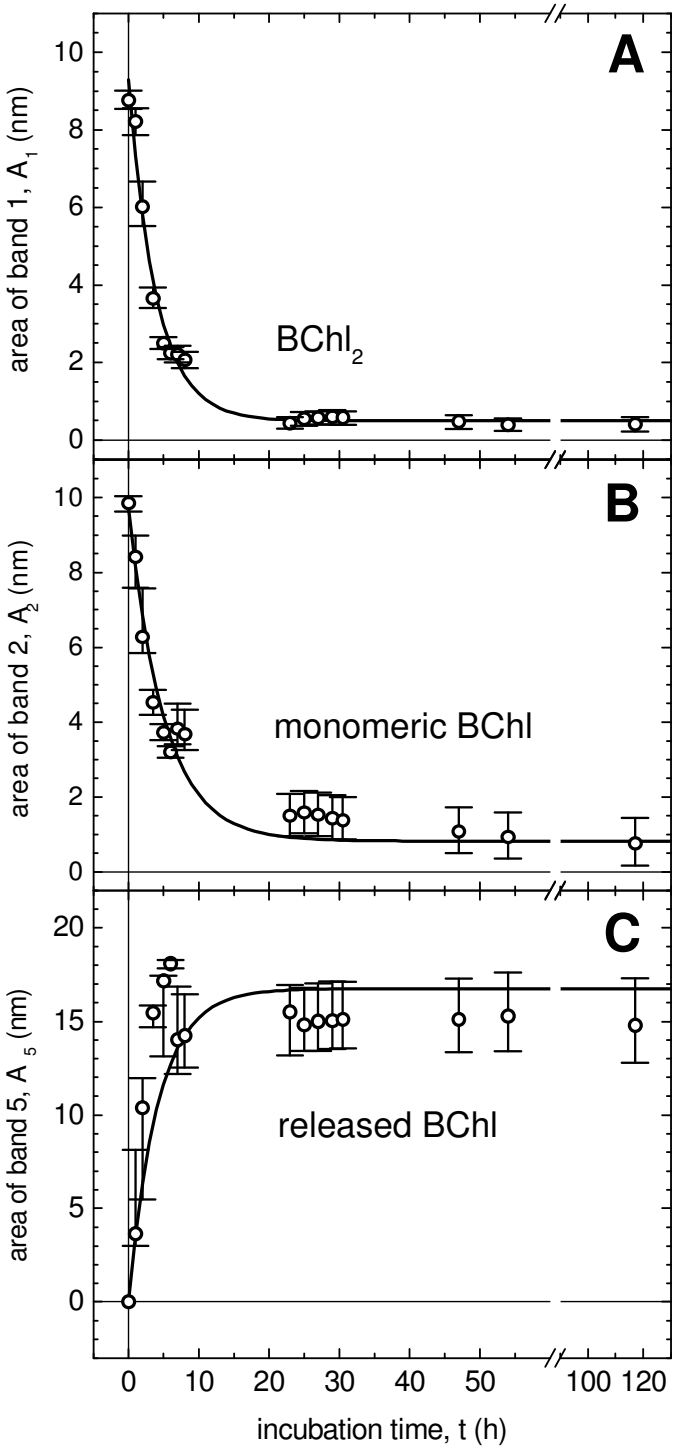
A
B
C
area of band 1, A1 (nm)
area of band 2, A2 (nm)
area of band 5, A5 (nm)
BChl2
monomeric BChl
released BChl
incubation time, t (h)
0
10
20
30
40
50
100
120

Figure 9

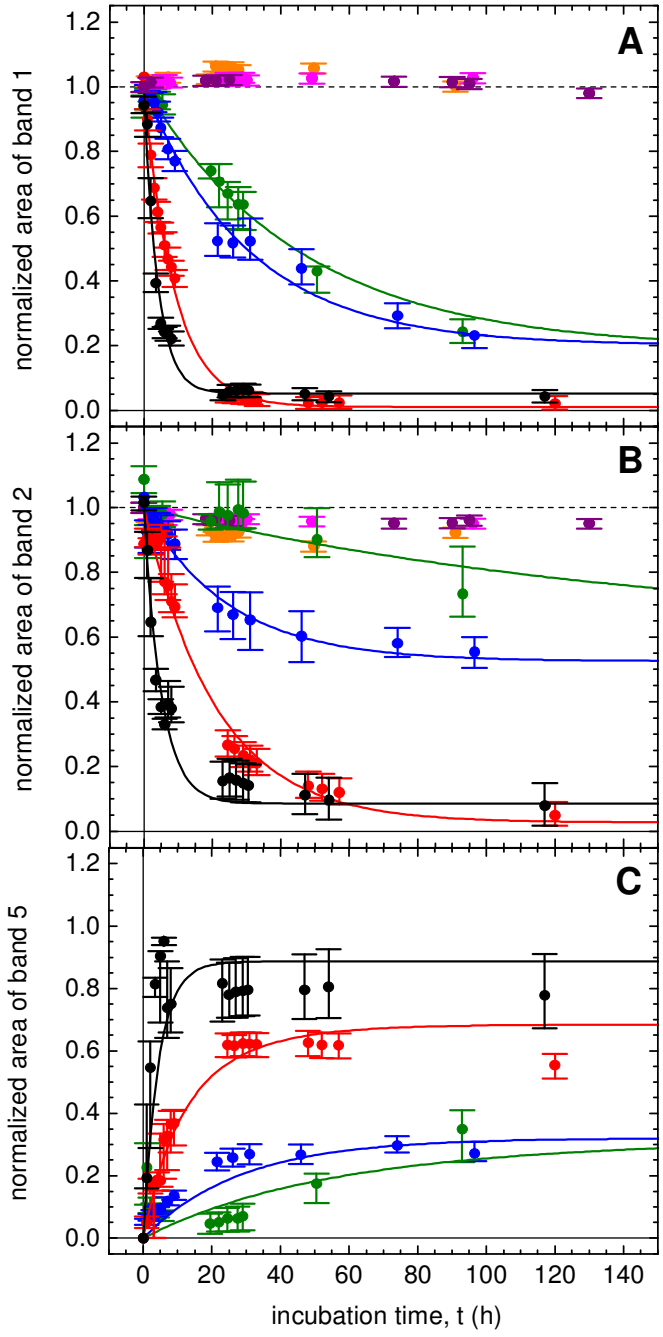
A
B
C
normalized area of band 1
normalized area of band 2
normalized area of band 5
incubation time, t (h)
0.0
0.2
0.4
0.6
0.8
1.0
1.2
0
20
40
60
80
100
120
140

Figure 10

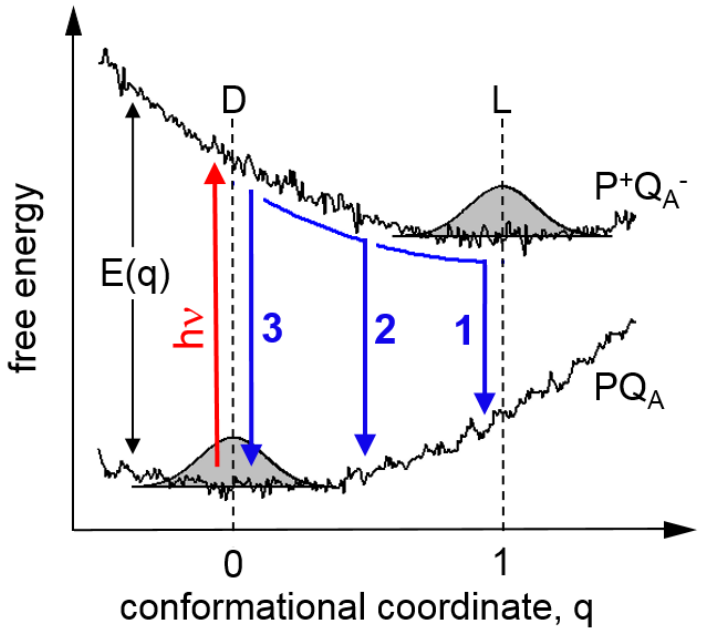
free energy
D
L
P+QA-
E(q)
hν
3
2
1
PQA
0
1
conformational coordinate, q

Table of Contents (TOC) Image